AIAA SciTech Forum
January 3-7, 2022, San Diego, CA & Virtual
AIAA SCITECH 2022 Forum

10.2514/6.2022-2253

Check for updates

Assessment of PAH-Based Precursor Models Using a Seven-Moment Quadrature-Based Closure for Soot Formation Prediction in Non-Premixed Laminar Flames

Jacques Xing* and Clinton P. T. Groth†

University of Toronto Institute for Aerospace Studies
4925 Dufferin Street, Toronto, Ontario, M3H 5T6, Canada

Downloaded by Clinton Groth on January 1, 2022 | http://arc.aiaa.org | DOI: 10.2514/6.2022-2253

The accurate numerical prediction of soot formation in practical combustion devices remains an open challenge. A recently proposed and computationally efficient quadrature-based moment closure based on fractional-order moments of soot particle volume, which is also capable of both capturing the polydispersity and key structural features of soot aggregates, is used here to explore the influence of the choice of polycyclic aromatic hydrocarbons (PAH)-based soot precursors on the formation, evolution, and oxidation of soot in ethylene-air laminar diffusion flames at atmospheric pressures. In particular, a seven-moment Conditional Quadrature Method of Moments (CQMOM) with a fixed quadrature point at the soot particle inception size, resulting in a so-called CQMOM-Radau closure, is used to explore the influence of the choice of soot precusors on soot formation prediction in laminar diffusion flames at atmospheric pressures. The CQMOM-Radau closure of interest involves the solution of a relatively small system of seven moment equations describing the soot transport but yet allows for a bivariate treatment and detailed modelling of the gas-phase chemistry along with treatments for soot particle nucleation, condensation, surface growth, oxidation, coagulation, sintering, obliteration, and fragmentation. The soot formation predictions of the seven-moment closure obtained using several PAH-based soot precursor models are investigated and compared to predictions obtained using a standard acetylene-based two-equation model, as well as available experimental data, for several atmospheric pressure laminar co-flow diffusion flames with ethylene as the fuel. The relative performances of the various PAH-based precursors for predicting the observed soot concentrations, particles sizes, and structure are discussed.

I. Introduction

I.A. Motivation

The inception and formation of soot particles in chemically reactive flows is known to depend on the presence of various chemical species referred to as precusors. These precursors may depend on the components of the fuel as well as flow conditions and various gaseous species have been suggested as possible choices for the precursors in the numerical modelling of soot formation in non-premixed laminar diffusion flames. In many early studies of soot formation, acetylene was taken to be the sole precusor for soot inception.[1–3] These early studies generally adopted simplified, semi-empirical, two-equation models for soot formation and the use of acetelyne-based inception models permitted significant simplifications in the associated models for the gas-phase chemical kinetics and soot chemistry. Unfortunately, acetelyne-based inception models cannot accurately represent the polydisperse and aggregrate nature of the soot particles and are well known to significantly underpredict soot volume fraction along the centerline of laminar co-flow diffusion flames.[4]

*Ph. D. Candidate, Email: jacques.xing@mail.utoronto.ca
†Professor, Email: groth@utias.utoronto.ca, AIAA Associate Fellow.

Copyright © 2022 by the American Institute of Aeronautics and Astronautics, Inc. All rights reserved.

More recent studies have established an interplay between soot formation and the presence of polycyclic aromatic hydrocarbons (PAH) and PAH-based inception models have been shown to provide significant improvements in the prediction of soot concentrations. However, while four-ring pyrene (A4) molecules have been widely used as a precursor in soot models,[5–7] there is however yet no strong consensus of which PAH species should be used as precursors for the accurate prediction of soot formation in laminar flames. For example, a five-ring PAH model, considering of BAPYR (benzo(a)pyrene), BAPYR*S (benzo(a) pyrenyl), and BGHIF (benzo(ghi)fluoranthene), was proposed and used by Eaves *et al.*[8] PAH precursors ranging up to 5-ring species were also recently examined by Jerez *et al.*,[4] and Wang *et al.*[9] considered a multi-PAH inception models with PAH species ranging from pyrene up to the seven-ring coronene (A7).

The uncertainties and complexities related to the modelling of soot precusors and chemistry is made further difficult by the polydisperse nature of the soot aggregates. In particulary, the evolution of soot particle size distribution is governed by a high-dimensional integro-differential population balance equation (PBE). In the PAH-based precursor studies described above, sectional methods[10–12] are very often used to solve the PBE. Unfortunately, a rather high number of sections is generally required to ensure reasonable accuracy for engineering accuracy and such techniques may not be feasible for practical simulations. Alternatively, the method of moments[13–18] requires the solution of only a small number of transport equations for moments of the soot particle distribution function and represents a good comprise between accuracy and computational cost. It is therefore potentially better suited to practical flame simulations for engineering applications.

Notably, Quadrature Method of Moments (QMOM) represent the distribution function as a sum of Dirac delta functions or a sum of products of Dirac detla functions and can be used for both univariate[15,19–21] or bivariate[22] descriptions. The source terms of the moment transport equations can then be closed rather efficiently by direct quadrature. For the univariate case, the weights and abscissa of the Dirac functions of the basic QMOM approach are computed from the know moments by a set of non-linear equations that can be solved by the product-difference algorithm (PDA)[23] or the Wheeler[24] algorithm. However, the basic QMOM approach is difficult to extend to multivariate problems because of the complexity of the inversion problem requiring advanced computational methods such as conjugate-gradient minimization algorithm.[22] A variant of the QMOM approach which consists of directly solving for the weights and the abscissa of the Dirac functions is referred to as Direct Quadrature Method of Moments (DQMOM)[25,26] and has the advantage that it can be readily extended to multivariate problems.[26–29] While DQMOM[30–36] has been used for soot modelling, the approach is not fully conservative without a specific treatment of the convective fluxes in multi-dimensional problems.[37] In addition, the approach requires the inversion of an ill-conditionned matrix and becomes unstable when the quadrature abscissa are not distinct. However, the inversion problem for multivariate QMOM description can also be simplified by the Conditional Quadrature Method of Moments (CQMOM),[29,37–40] which represents the multivariate density distribution as a product of conditional density functions.

Recently, Xing *et al.*[41] have proposed both univariate Quadrature Method of Moments (QMOM) and bivariate Conditional Quadrature Method of Moments in terms of fractional-order soot particle size moments with fixed quadrature points at the soot particle inception size, so-called QMOM-Radau and CQMOM-Radau moment closures, and have shown that such closures can significantly improve the accuracy of the prediction of number density and volume fraction. These recently proposed quadrature-based moment closures involve the solution of just a small system of moment equations (5 and 7 equations for the QMOM-Radau and CQMOM-Radau closures, respectively) while also readily allowing for the incorporation of detailed and consistent models of the soot physical and chemical kinetics, including PAH-based nucleation, PAH condensation, surface growth, oxidation, aggregation, obliteration, sintering, and fragmentation.

I.B. Scope of Present Study

The objective of this study is to examine the effects of the choice of PAH precursors on the prediction of soot formation in laminar ethylene diffusion flames by using the seven-moment fractional-order CQMOM-Radau closure of Xing *et al.*[41] For these purposes, both the Santoro burner[42] and the Smooke-Long (or Yale) burner[10] are considered in this study. However, the choice of PAH species that can be considered in the numerical simulations of soot formation depends highly on the choice of the chemical mechanism. Accordingly, the mechanism of Slavinskaya *et al.*,[43] which considers molecular growth up to 5-ring aromatics, is used in this study. This mechanism has been used in several previous numerical studies of the Santoro burner.[7,44,45] In the present study, a range of PAH species from the two-ring napthalene to five-ring PAHs will be considered. Additionally, the PAH-based inception results obtained with the CQMOM-Radau model

Downloaded by Clinton Groth on January 1, 2022 | http://arc.aiaa.org | DOI: 10.2514/6.2022-2253

are compared to results obtained using the semi-empirical two-equation model of Liu *et al.*[3]

II. Soot Modelling

II.A. Soot Aerosol Modelling

II.A.1. Semi-Empirical Two-Equation Models

Standard semi-empirical two-equation models[1–3,46–51] solve transport equations for the soot number density per unit mass, N_s, and the soot mass fraction, Y_s,

$$\frac{\partial}{\partial t}(\rho N_s) + \frac{\partial}{\partial x_j}\left[\rho N_s(u_j + V_{T,j})\right] = S_{N_s}, \tag{1}$$

$$\frac{\partial}{\partial t}(\rho Y_s) + \frac{\partial}{\partial x_j}\left[\rho Y_s(u_j + V_{T,j})\right] = S_{Y_s}, \tag{2}$$

where ρ is the mixture density, u_j is the flow velocity, and $V_{T,j}$ is the thermophoretic velocity. The number density source term, S_{N_s}, and the mass fraction source term, S_{Y_s}, are respectively evaluated using

$$S_{N_s} = \frac{2}{C_{\min}} N_A \bar{R}_{\text{nuc}} - 2C_{\text{coag}}\left(\frac{6k_B T}{\rho_s}\right)^{1/2} d_p^{1/2}(\rho N_s)^2 \tag{3}$$

and

$$S_{Y_s} = 2M_s(\bar{R}_{\text{nuc}} + \bar{R}_{\text{sg}}) - M_s\bar{R}_{\text{ox}}, \tag{4}$$

where M_s is the molar mass of the soot, taken to be the molar mass of carbon, N_A is the Avogadro number, k_B is the Boltzmann constant, T is the gas temperature, ρ_s is the soot particle density, $C_{\min}$ is the number of carbon atoms of the incipient soot particles, C_{coag} is an empirical coefficient for the coagulation rate, and d_p is the diameter of the soot particles. The molar nucleation rate, $\bar{R}_{\text{nuc}}$ [kmol/m^3/s], the molar surface growth rate, $\bar{R}_{\text{sg}}$ [kmol/m^3/s], and the molar oxidation rate, $\bar{R}_{\text{ox}}$ [kmol/m^3/s], are given by

$$\bar{R}_{\text{nuc}} = k_{\text{nuc}}[\text{C}_2\text{H}_2], \tag{5}$$

$$\bar{R}_{\text{sg}} = k_{\text{sg}} A_s^{n_s}[\text{C}_2\text{H}_2], \tag{6}$$

$$\bar{R}_{\text{ox}} = (2k_{\text{ox,O}_2}[\text{O}_2] + k_{\text{ox,OH}}[\text{OH}] + k_{\text{ox,O}}[\text{O}])A_s, \tag{7}$$

respectively, while the primary particle diameter, d_p, and total surface area, A_s, are given respectively by

$$d_p = \left(\frac{6M_s}{\pi\rho_s}\right)^{1/3}[\text{C(s)}]^{1/3}(\rho N_s)^{-1/3}, \tag{8}$$

and

$$A_s = \pi\left(\frac{6M_s}{\pi\rho_s}\right)^{2/3}[\text{C(s)}]^{2/3}(\rho N_s)^{1/3}, \tag{9}$$

where [C(s)], [C_2H_2], [O_2], [OH], and [O] are respectively the soot, C_2H_2, O_2, OH, and O molar concentrations while k_{nuc}, k_{sg}, $k_{\text{ox,O}_2}$, $k_{\text{ox,OH}}$, and $k_{\text{ox,O}}$ are respectively reaction rate coefficients for nucleation, surface growth, oxidation by O_2, oxidation by OH, and oxidation by O. Finally, n_s is an empirical surface exponent for surface growth.

II.A.2. Seven-Moment Fractional-Order CQMOM-Radau Moment Closures

In the Hybrid Method of Moments (HMOM), Mueller *et al.*[14] introduced a quadrature point or abscissa, V_0, that was held fixed to represent the volume associated with newly created soot particles at inception. More recently, for the QMOM, Salenbauch *et al.*[17] similarly suggested fixing one abscissa, V_0, at specific size related to inception and thereby only requiring the solution for the corresponding weight N_0. Applying

Downloaded by Clinton Groth on January 1, 2022 | http://arc.aiaa.org | DOI: 10.2514/6.2022-2253

the same approach with CQMOM, a so-called CQMOM-Radau moment closure is obtained. In the bivariate quadrature-based moment closure descriptions for soot transport as proposed by Xing *et al.*,[41] the soot aerosols are represented as polydisperse fractal-like aggregates consisting of linked chain-like structures of primary particles. As such, the proposed bivariate description uses the aggregate volume, V, and the number of primary particles, n_p, making up the soot aggregates (the latter are assumed to consist of multiple primary particles). The form of the approximate distribution function in the quadrature-based moment closure with a fixed quadrature at the inception size is then given by

$$n(V, n_p) = N_0 \delta(V - V_0)\delta(n_p - 1) + \sum_{i=1}^{N_V - 1} \sum_{j=1}^{N_{n_p}} N_{i,j} \delta(V - V_i)\delta(n_p - n_{p_{i,j}}) \,, \tag{10}$$

where $N_{i,j}$ represents the quadrature density number, V_i are the aggregate volume quadrature points, and $n_{p_{i,j}}$ are the conditional primary particle number quadrature points. Additionally, N_V is the number of volume Dirac functions used in the quadrature-based description and N_{n_p} is the number of Dirac functions for primary particle number. The bivariate moments, $M_{k,l}$ are then given by

$$M_{k,l} = N_0 V_0^k + \sum_{i=1}^{N_V - 1} \sum_{j=1}^{N_{n_p}} N_{i,j} V_i^k n_{p_{i,j}}^l . \tag{11}$$

Transport equations are then solved for a total of $2N_V - 1 + (N_V - 1)(2N_{n_p} - 1)$ bivariate moments

$$\frac{\partial}{\partial t}(M_{k,l}) + \frac{\partial}{\partial x_j}\left[M_{k,l}(u_j + V_{T,j})\right] = \dot{M}_{k,l}, \tag{12}$$

with $\dot{M}_{k,l} = \dot{M}_{k,l,\text{nuc}} + \dot{M}_{k,l,\text{sg}} + \dot{M}_{k,l,\text{ox}} + \dot{M}_{k,l,\text{coag}} + \dot{M}_{k,l.\text{cond}} + \dot{M}_{k,l,\text{sint}} + \dot{M}_{k,l,\text{frag}}$, where $\dot{M}_{k,l,\text{nuc}}$, $\dot{M}_{k,l,\text{sg}}$, $\dot{M}_{k,l,\text{ox}}$, $\dot{M}_{k,l,\text{coag}}$, $\dot{M}_{k,l,\text{cond}}$, $\dot{M}_{k,l,\text{sint}}$, and $\dot{M}_{k,l,\text{frag}}$ are source terms associated with nucleation, surface growth, oxidation, coagulation, condensation, sintering, and fragmentation, respectively. Those source terms are computed via direct numerical quadratures from the quadrature weights, $N_{i,j}$, and the quadrature abscissa, V_i and $n_{p_{i,j}}$, obtained from the inversion of the transported moment sets, $M_{k,l}$.

While originally developed for integer-order moments, the CQMOM-Radau closure can be extended to fractional-order moments by introducing a variable change and expressing the moments as

$$\begin{aligned} M_{k,l} = M_{x/k_V, y/l_{n_p}} &= N_0 V_0^{x/k_V} n_{p_0}^{y/l_{n_p}} + \sum_{i=1}^{N_V - 1} \sum_{j=1}^{N_{n_p}} N_{i,j} V_i^{x/k_V} n_{p_{i,j}}^{y/l_{n_p}} \\ &= N_0 \tilde{V}_0^x \tilde{n}_{p_0}^y + \sum_{i=1}^{N_V - 1} \sum_{j=1}^{N_{n_p}} N_{i,j} \tilde{V}_i^x \tilde{n}_{p_{i,j}}^y , \end{aligned} \tag{13}$$

where x and y are integer-order moments while k_V and l_{n_p} are the fraction denominators. The fractional-order formulation of Eqs. (13) reduces to integer order for $k_V = 1$ and $l_{n_p} = 1$. Xing *et al.*[41] have demonstrated via comparisons with results from a sectional method that 1/3-fractional-order volume moments ($k_V = 3$) can significantly improves the prediction of soot volume fraction and density number. Thus, a seven-moment CQMOM-Radau closure is considered here where the moment set includes the following moments: $M_{0/3,0}$, $M_{1/3,0}$, $M_{2/3,0}$, $M_{1,0}$, $M_{4/3,0}$, $M_{0,1}$, and $M_{1/3,1}$. Those moments can then be related to several physical quantities such as density number, N, soot volume fraction, f_V, primary particle density number, N_p, mean aggregate volume, $\bar{V}$, mean primary particle per aggregate, n_p, and mean volume-equivalent diameter, $\bar{d}_v$,

$$N = M_{0,0} \,, \quad f_V = M_{1,0} = N\bar{V} \,, \quad N_p = M_{0,1} = N\bar{n}_p \,, \quad \bar{V} = \frac{M_{1,0}}{M_{0,0}} \,, \quad \bar{n}_p = \frac{M_{0,1}}{M_{0,0}} \,, \quad \bar{d}_V = \left(\frac{6}{\pi}\right)^{1/3} \frac{M_{1/3,0}}{M_{0,0}} \,, \tag{14}$$

while other moments can be related to the standard deviation, σ_{d_V}, skewness, s_{d_V}, and kurtosis, κ_{d_V}, of the volume-equivalent diameter

$$\left(\frac{6}{\pi}\right)^{2/3} M_{2/3,0} = N\bar{d}_V^2 + N\sigma_{d_V}^2 \,, \quad \left(\frac{6}{\pi}\right) M_{1,0} = N\bar{d}_V^3 + 3N\bar{V}\sigma_{d_V}^2 + N s_{d_V} \,, \tag{15}$$

$$\left(\frac{6}{\pi}\right)^{4/3} M_{4/3,0} = N\bar{d}_V^4 + 6N\bar{V}^2\sigma_{d_V}^2 + 4N\bar{d}_V s_{d_V} + N\kappa_{d_V} \,. \tag{16}$$

Downloaded by Clinton Groth on January 1, 2022 | http://arc.aiaa.org | DOI: 10.2514/6.2022-2253

Table 1. PAH precursors used with the mechanism of Slavinskaya *et al.*[43]

4-ring[5–7,17,52–56]	Pyrene (A_4)
4-ring (Zhang *et al.*, 2019)[57]	Naphthalene (A_2), Acenaphthylene (A_2R_5), Phenanthrylacetylen (A_3C_2H), Pyrene (A_4) Benzo[ghi]fluoranthene (BGHIF)
5-ring (Eaves *et al.*, 2015)[44]	Benzo[ghi]fluoranthene (BGHIF) Benzo[a]pyrene, Benzo[a]pyrenyl
5-ring (Eaves *et al.*, 2017)[45]	Naphthalene (A_2), Acenaphthylene (A_2R_5), Biphenyl (P_2), Phenanthrene (A_3), Pyrene (A_4), Ethynyl pyrene (A_4C_2H), Benzo[ghi]fluoranthene (BGHIF), Benzo[a]pyrene

Downloaded by Clinton Groth on January 1, 2022 | http://arc.aiaa.org | DOI: 10.2514/6.2022-2253

II.B. Soot Chemistry Modelling

The semi-empirical two-equation model of Liu *et al.*[3] considers acetylene-based nucleation with $C_{\min} = 700$ and surface growth with an empirical surface exponent $n_s = 0.5$. An oxidation efficiency of 0.2 is used for oxidation by OH and O while oxidation by O_2 is modelled by the Nagle/Strickland-Constable (NSC) multi-step reaction rate. In order to predict the evolution of primary particles, the coagulation term has been neglected ($C_{\text{coag}} = 0$). Consequently, the model of Liu *et al.*[3] is only able to track the evolution of the primary particle density number and primary particle size. Hence, the aggregate density number is not determined with such an approach. Additional details about this specific version of the semi-empirical two-equation model can be found in the original work of Liu *et al.*[3]

For the seven-moment CQMOM-Radau closure, the PAH species or species combinations that are considered herein are summarized in Table 1. Among the possible models, the 4-ring pyrene has been the most common choice in previous numerical studies on soot formation in laminar diffusion flames.[5–7,17,52–56] Alternatively, the PAH-based model of Zhang *et al.*[57] considers several PAHs smaller than pyrene while the model of Eaves *et al.* (2015)[44] is based on 5-ring PAHs. Finally, the model of Eaves *et al.* (2017)[45] considers both PAHs smaller than pyrene and 5-ring PAHs. The rate of inception is computed from the free-molecular collision kernel along with the nucleation efficiency model of Raj *et al.*[9,58] and an empirical factor $C_0 = 0.05$. The condensation rate is computed from the free-molecular kernel with a constant efficiency of 0.3[59–61] while the aggregation rate is computed from the kernel of Rogak and Flagan.[62] The relationships of Rogak and Flagan[62] are used to determine soot mobility diameters while the collision and the absorbing sphere diameters are computed from the approach of Zurita-Gotor and Rosner.[63] The outer diameter is computed from Naumann[64] with a filing factor $f = 1.43$ and a constant fractal dimension $D_f = 1.8$. The Cunningham slip factor is determine from the relationship of Phillips.[65] Surface growth is evaluated using the HACA mechanism of Blanquart and Pitsch[33] with a constant steric factor. The rate of oxidation by O_2 is modelled from Appel, Bockhorn and Frenklach[66,67] while an oxidation efficiency of 0.10 is assumed for oxidation by OH and O. In addition, obliteration due to surface growth and condensation is modelled from Rogak and Park.[68] Finally, the sintering rate is modelled by the approach of Veshkini *et al.*[69] while fragmentation rate is modelled by the approach of Mueller *et al.*[70]

III. Numerical Solution Method for Laminar Flames

III.A. Parallel Implicit Finite-Volume Scheme

Charest *et al.*[71] previously developed a computational framework for the prediction of soot formation in laminar diffusion flames. In this framework, the Navier-Stokes equations for two-dimensional, planar and axisymmetric, laminar flows of a multi-component gaseous mixture with detailed chemistry are discretized by a finite-volume method using a second-order piecewise limited reconstruction for the evaluation of inviscid fluxes and a diamond path is used for the evaluation of the viscous fluxes. Low-Mach preconditioning is introduced in order to reduce excessive numerical dissipation and numerical stiffness. Steady-state solutions

Table 2. Summary of the Santoro ethylene laminar diffusion burner.

Fuel tube extension	4.0 mm
Fuel tube diameter	11.1 mm
Coflow diameter	101.6 mm
Fuel mass flow	4.388 mg/s
Air mass flow	0.836 g/s
Pressure	1 atm
Fuel	C_2H_4

of the discrete solutions are obtained by an inexact Newton-Krylov-Schwarz (NKS) algorithm while radiative heat transfer is solved with discrete-ordinate-method (DOM) for a non-gray media. The computational framework of Charest *et al.*[71] has been used in a number of previous studies to predict soot formation in elevated pressure laminar diffusion flames for a variety of gaseous fuels ranging from ethylene,[72] methane,[73] and biogas.[74] The computational framework of Charest *et al.* was recently extended by Xing *et al.*[41] to allow for the treatment and solution of fractional-order quadrature-based moment closures for describing the soot aerosol dynamics. In order to preserve moment-realizability, the soot moment transport equations are discretized by using a first-order upwind finite-volume scheme for the convection. In addition, a Strang splitting is applied to the treatent of the source terms in the soot moment equations.

III.B. Numerical Setup for Laminar Co-Flow Flames

Numerical results for the sooting ethylene-fueled laminar flames associated with the Santoro[42] and Smooke-Long (or Yale) burners[10] are both considered in present study. The experimental data sets for both sets of flames are part of the laminar flames section of the International Sooting Flame (ISF) Workshop.[75]

III.B.1. Santoro Burner

The characteristics of the Santoro burner[42] are summarized in Table 2. The fuel tube has an inner diameter of 11.1 mm and extends 4.0 mm beyond the exit plane of the coflow tube. The latter has an inner diameter of 101.6 mm. Ethylene flows throught the fuel tube at a rate of 4.388 mg/s while the coflow air flows at a rate of 0.836 g/s. This configuration has been widely studied experimentally[76–83] and numerically.[6,8,44,45,52,69,84–86] Notably, a wide range of experimental data in terms of soot volume fraction, primary particle diameter, primary particle number, and aggregate number density is available in the literature. In this respect, the Santoro burner represents a good validation case for a bivariate soot model such as the proposed fractional-order CQMOM-Radau approach.

The pre-heating of the fuel stream can have an important impact on flame structure and soot formation. In this respect, various approaches have been proposed to take into consideration the pre-heating of the fuel stream. For example, Dworkin *et al.*[52] assumed an inlet temperature of 400 K while Veshkini *et al.*[69,86] assumed a much higher inlet temperature of 650 K based on the tip tube temperature measurements of Boedeker *et al.*[87] Alternatively, Eaves *et al.*[44,45] used conjugate heat transfer (CHT) to more accurately model the fuel pre-heating. However, in this study a different approach is used. Instead of assuming an uniform inlet temperature profile of 650 K for the fuel stream as in Veshkini *et al.*,[69,86] the 4.0 mm tube extension of the Santoro burner is modelled and a temperature of 650 K is only imposed on the tip of the tube. The fuel and coflow temperatures are respectively assumed to be 400 K and 300 K as recommended by the ISF Workshop.[75] In addition, consistent with the experimental data of Boedeker *et al.*,[87] a linear temperature profile is imposed along the tube wall from the coflow exit plane to the tip of the tube. A parabolic and an uniform velocity profiles are respectively assumed for the fuel stream and the coflow stream. Finally, a reflection boundary condition is applied on the centerline while the far-field boundary is treated using a free-slip condition. The various boundary conditions used have been summarized on Figure 1(a).

The two-dimensional axisymmetric computational domain used for the numerical calculations has a downstream length of 120 mm as suggested by the ISF Workshop[75] with a radius equals to 50.8 mm. The

Downloaded by Clinton Groth on January 1, 2022 | http://arc.aiaa.org | DOI: 10.2514/6.2022-2253

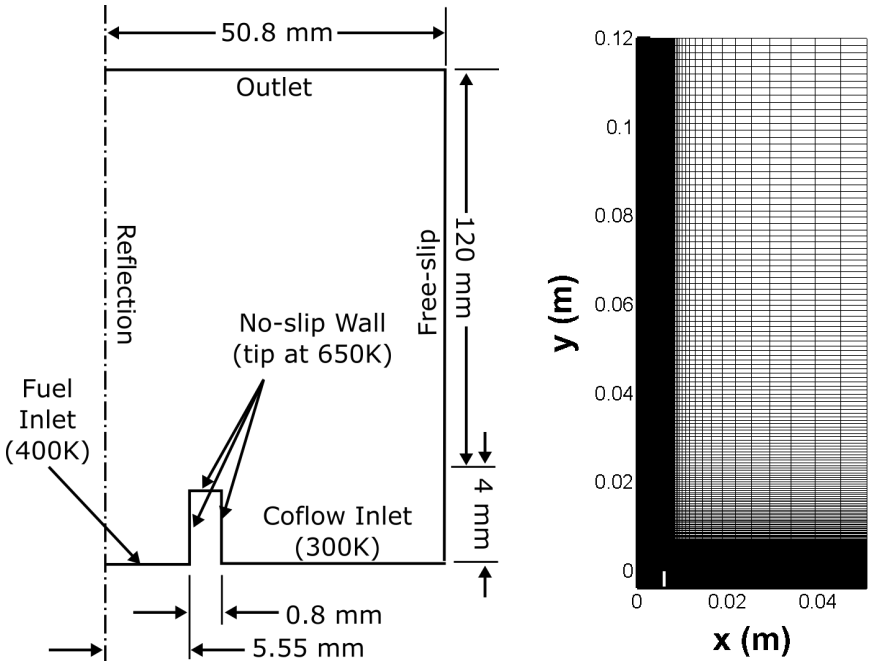

(a) Schematic diagram (b) Computational grid

Figure 1. Schematic diagram and two-dimensional axisymmetric computation grid for the Santoro laminar diffusion flame.

Table 3. Summary of the Smooke-Long coflow laminar diffusion flame.

Fuel tube inner diameter	4.0 mm
Fuel tube thickness	0.38 mm
Coflow inner diameter	50.0 mm
Fuel mass flow	5.003 mg/s
Air mass flow	0.804 g/s
Pressure	1 atm
Fuel	32%, 40%, 60%, and 80% C_2H_4

computational domain shown on Figure 1(b) is divided in 192 cells in the radial direction and in 320 cells in the axial direction for a total of 61 440 cells. Solutions are obtained with the NKS with low-Mach preconditioning while radiative heat transfer is modelled with DOM and the T_3[88] quadrature rule along with statistical narrow band correlated-k (SNBCK)[89] using $N_b = 9$ bands with $N_g = 4$ Gauss-quadrature points. Finally, an efficiency of 0.20 is used here to model soot aggregation as in many previous numerical studies of the Santoro burner.[8,69,85,86] In addition, an unity steric factor for the HACA surface growth is assumed here.

III.B.2. Smooke-Long Burner

The Smooke-Long burner[10] has been used to generate atmospheric pressure ethylene coflow diffusion flames at various dilution levels and has been the subject of many experimental[10,90–105] and numerical[10,90–93,103,105,106] studies. The characteristics of the Smooke-Long burner are summarized in Table 3. The fuel tube has an inner diameter of 4.0 mm with a wall thickness of 0.38 mm while the coflow tube has an inner diameter of 50.0 mm. Ethylene with nitrogen dilution flows throught the fuel tube at a combined rate of 5.003 mg/s while the coflow air flows at a rate of 0.804 g/s. The various levels of dilution that have been considered correspond to ethylene concentration of 32%, 40%, 60%, and 80%.

Downloaded by Clinton Groth on January 1, 2022 | http://arc.aiaa.org | DOI: 10.2514/6.2022-2253

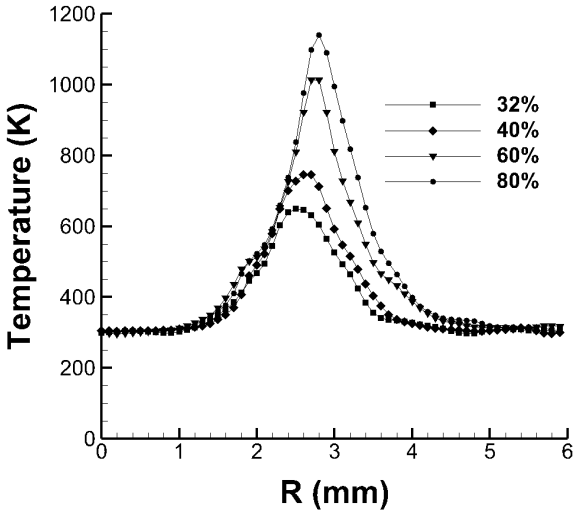

Figure 2. Inlet temperature profiles for the Smooke laminar diffusion flame for each ethylene concentration (32%, 40%, 60%, and 80%). Experimental data from Kempema *et al.*[100]

Downloaded by Clinton Groth on January 1, 2022 | http://arc.aiaa.org | DOI: 10.2514/6.2022-2253

A parabolic and an uniform velocity profiles are respectively assumed here for the fuel and coflow streams as in McEnally *et al.*[90] In contrast to the Santoro burner case, the experimental temperature profiles of Kempema *et al.*[100] are imposed as boundary condition at the inlet. Figure 2 shows the inlet temperature profile for each dilution level. Again, a reflection boundary condition is applied along the centerline while the far-field boundary is treated using a free-slip condition. The various boundary conditions are summarized on Figure 3(a).

As recommended by the ISF Workshop,[75] the two-dimensional axisymmetric computational domain extends 70, 80, 100, and 120 mm downstream the inlet respectively for the cases with 32%, 40%, 60%, and 80% ethlyene while the domain radius is set equal to 75.0 mm. An example of the computational grid for the case with 80% ethlyene is shown on Figure 3(b). For all ethylene concentration levels, the computational domain is divided in 192 cells in the radial direction and in 320 cells in the axial direction for a total of 61 440 cells. The governing equations are solved with the NKS with low-Mach preconditioning. The radiative heat transfer is modelled with DOM and T_3[88] quadrature rule along with SNBCK[89] using $N_b = 9$ bands with $N_g = 4$ Gauss-quadrature points. As reduced soot reactivity with dilution levels has been previously observed and reported by Veshkini *et al.*[7] and by Khosousi and Dworkin,[107] different values of steric factor, α_s, are used for each dilution level. Hence, in this study steric factors of 0.2, 0.5, 0.8, and 1.0 are respectively used for the case with 32%, 40%, 60%, 80% ethylene. Finally, an unity aggregation efficiency is assumed here.

IV. Numerical Results

The numerical simulation results and predictions of soot formation for the laminar co-flow diffusion flames of both the Santoro and Smooke-Long burners are now discussed.

IV.A. Santoro Burner Laminar Co-Flow Diffusion Flames

IV.A.1. Validation of Flame Structure

The ability of the choices of chemical mechanism and boundary conditions used in the numerical simulations to properly predict the flame temperature and structure is first verified here. Comparisons of radial and centerline temperature profiles with the experimental data of Santoro *et al.*[76] and of the ISF Workshop[75] are shown on Figure 4. The results indicate that overall the radial temperature profiles are well reproduced by all precursor models with some underprediction near the centerline at lower axial positions. However, the centerline temperature profile appears to be slightly shifted downstream which explains the underprediction of centerline temperature at lower axial locations. While the results indicate that some improvements

Downloaded by Clinton Groth on January 1, 2022 | http://arc.aiaa.org | DOI: 10.2514/6.2022-2253

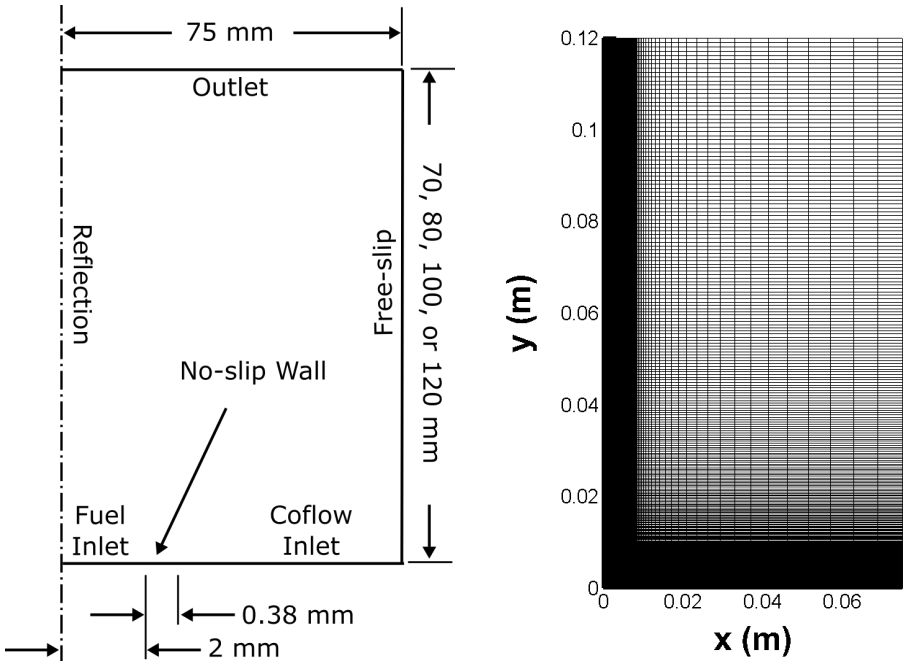

(a) Schematic diagram (b) Computational grid

Figure 3. Schematic diagram and two-dimensional axisymmetric computation grid for the Smooke laminar diffusion flame.

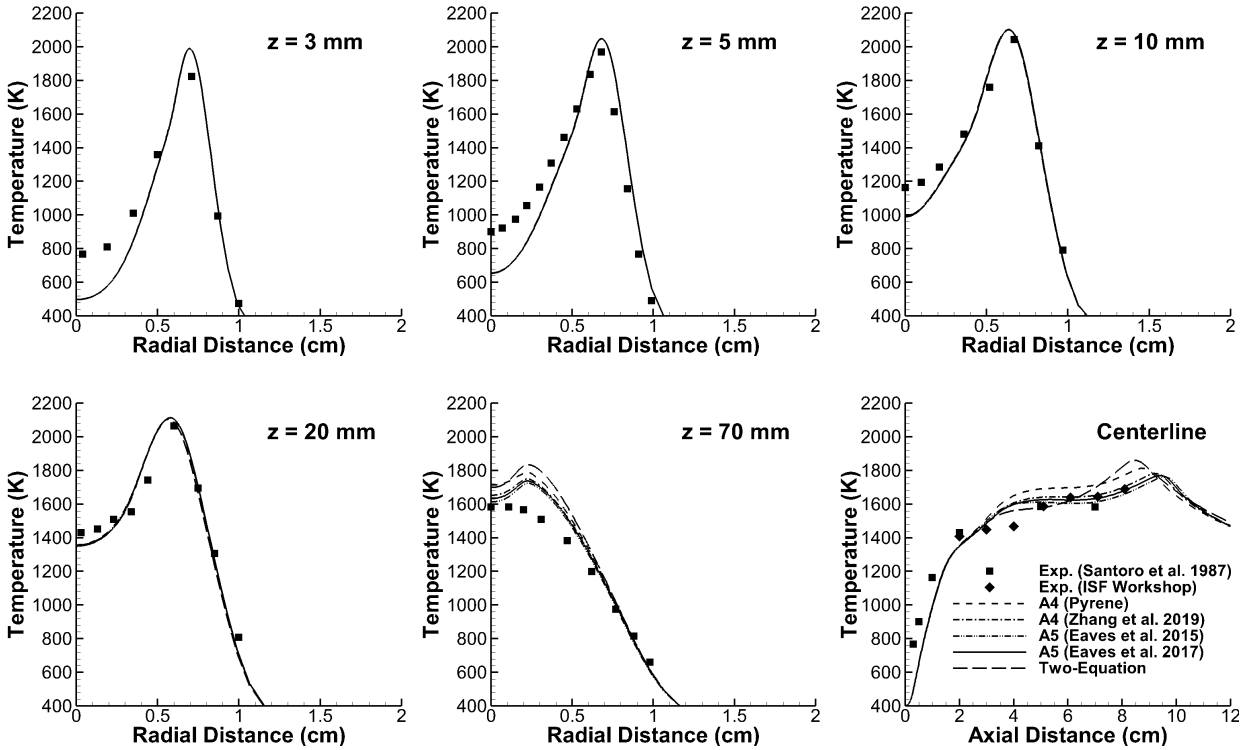

Figure 4. Radial and centerline temperature profiles for the Santoro laminar diffusion flame. Experimental data from Santoro *et al.*[76] and the ISF Workshop.[75]

could still be obtained by considering CHT, this is left for future studies as the results obtained here are deemed to be sufficiently accurate. It can also be seen that there are differences in the predicted centerline

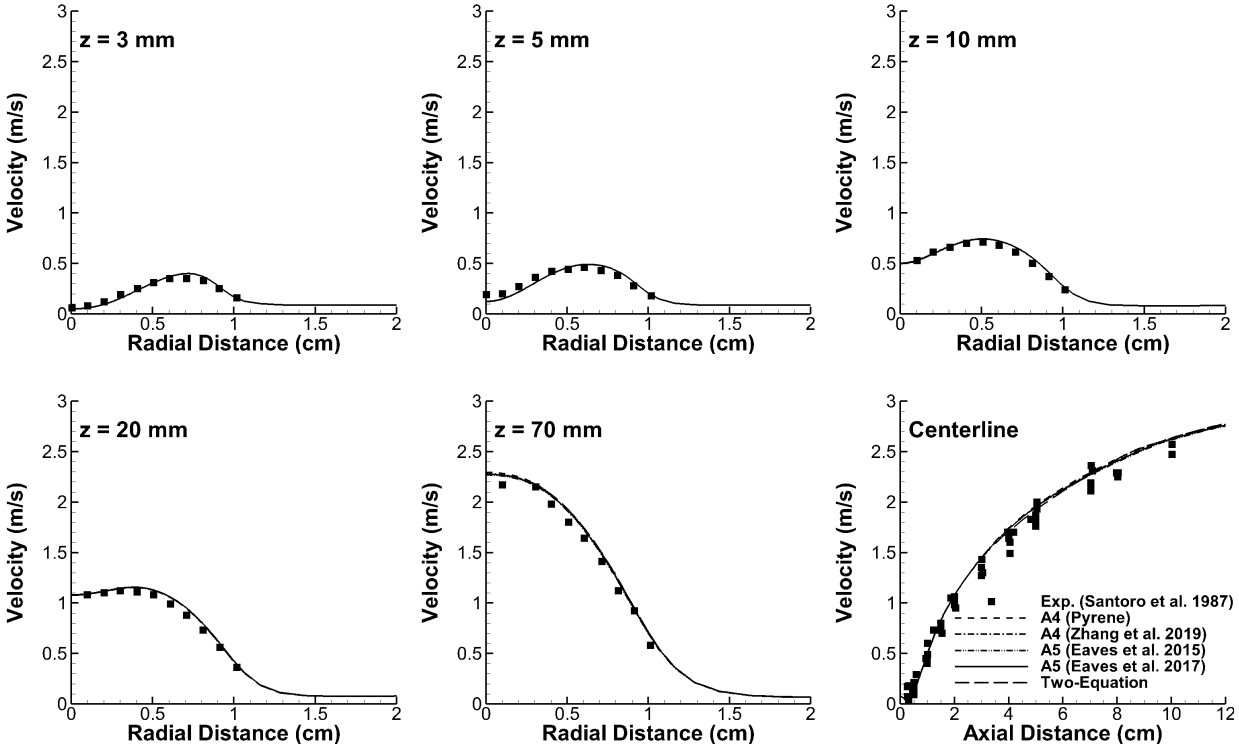

Figure 5. Radial and centerline velocity profiles for the Santoro laminar diffusion flame. Experimental data from Santoro *et al.*[76]

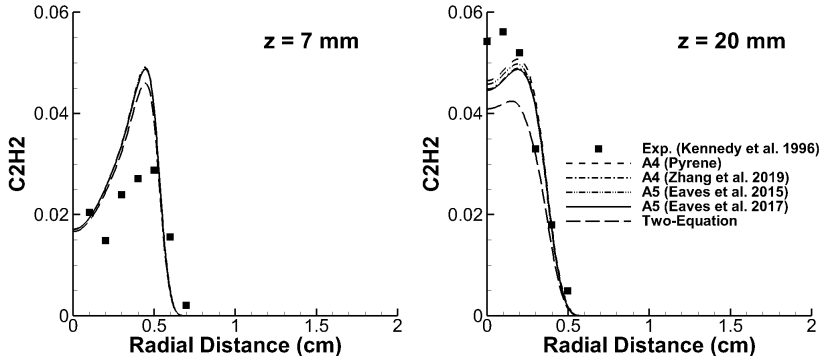

Figure 6. Radial profiles of C_2H_2 mass fraction for the Santoro laminar diffusion flame. Experimental data from Kennedy *et al.*[80]

temperature profiles between the various precursor models. Those discrepancies are explained by differences in the predicted soot volume fraction which subsequently affects the radiative heat loss.

Radial and centerline velocity profiles are well predicted comparatively to the experimental data of Santoro *et al.*[76] for all precursors considered as shown on Figure 5. Notably, the magnitude and the location of the maximum velocity are well captured for all axial locations and the choice of precursors has a minimal impact on velocity profiles. Next, the predicted C_2H_2 and OH mass fractions are compared to the experimental data of Kennedy *et al.*[80] Regarding the C_2H_2 mass fraction, Figure 6 shows a moderate overprediction at z = 7 mm with an excellent prediction at z = 20 mm. Accurate predictions of C_2H_2 mass fraction is of great importance since it is one of the main source of soot particles growth. Results also show some sensitivity to the precursor models which is expected since the formation of soot particles, and hence the consumption of C_2H_2, is affected by the choice of inception and/or condensation models. Finally, Figure 7 indicates that the OH mass fraction is well predicted at both z = 7 mm and z = 70 mm in terms of both

Downloaded by Clinton Groth on January 1, 2022 | http://arc.aiaa.org | DOI: 10.2514/6.2022-2253

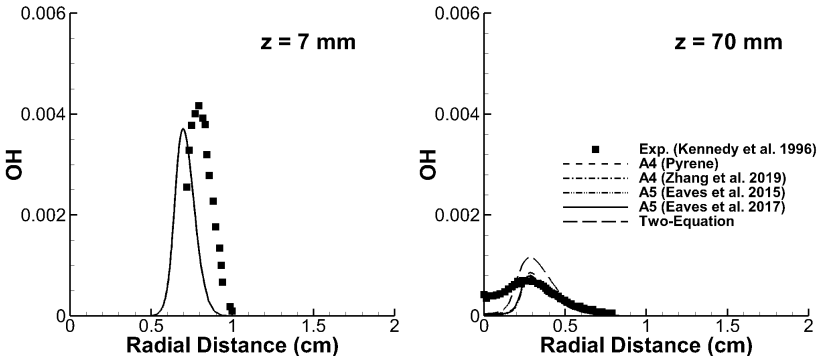

Figure 7. Radial profiles of OH mass fraction for the Santoro laminar diffusion flame. Experimental data from Kennedy *et al.*[80]

the location and the magnitude of the peak concentration.

IV.A.2. Effects of PAH Precursors on Soot Formation

Figure 8 compares the radial and the radially integrated soot volume fraction with the experimental data of McEnally *et al.*[81] and of Kennedy *et al.*[80] Results indicate that the two-equation model of Liu *et al.*[3] significantly underpredicts the soot volume fraction along the centerline and overpredicts the peak soot volume fraction along the wings at lower axial distances. Similarly, the pure pyrene model also results in an underprediction of soot soot volume fraction along the centerline. However, noticeable improvements can be observed when additional PAHs are considered in the inception and condensation models. In addition, results indicate that the radially integrated soot volume fraction is well predicted by the CQMOM-Radau models with excellent results obtained from the 5-ring model of Eaves *et al.* (2015)[44] and a moderate underprediction with the pure pyrene model. In comparison, the two-equation model of Liu *et al.*[3] overpredicts the integrated soot volume fraction and predicts an early peak.

Figure 9 shows the soot volume fraction, mean primary particle diameter, mean primary particle number, aggregate number density, and primary particle number density along the line of maximum soot volume fraction. Results indicate that while the radially integrated soot volume fraction is well predicted by PAH-based models, the peak soot concentration is underpredicted comparatively to the experimental data of Megaridis and Dobbins[78] and of McEnally *et al.*[81] In particular, the pure pyrene model shows significant underprediction of peak soot volume fraction. Consequently, the contribution to the total soot volume fraction from other PAH molecules can be non-negligible. On the other hand, the two-equation model of Liu *et al.*[3] better predicts the peak soot volume fraction although with a premature peak location. Nevertheless, the good performances of this model can be explained because it has been specially calibrated for ethylene flames.

Figure 9 also indicates that the mean primary particle diameter is well predicted by all PAH precursor models despite the fact that the numerical results are slightly shifted downstream comparatively to the experimental data of Megaridis and Dobbins[78] and of Iyer *et al.*[83] Good prediction of mean primary particle diameter is also obtained with the two-equation model of Liu *et al.*[3] On the other hand, Figure 9 shows that considering smaller PAHs (models of Zhang *et al.*[57] and of Eaves *et al.* (2017)[45]) results in an early inception of soot particles as indicated by the additional peak of mean primary particle number. Figure 9 shows as well that the aggregate number density is relatively well predicted by all PAH models comparatively to the experimental data of Santoro *et al.*[76] Additionally, it should be noted that the increase of aggregate number density from a distance of about 8.0 cm above the burner is due to oxidation-induced fragmentation. However, the absence of experimental data prevents the validation of the fragmentation model. Regarding the two-equation model of Liu *et al.*,[3] neither the mean primary particle number nor the aggregate number density can be predicted since the model only tracks the primary particle number density by neglecting aggregation. Finally, all approaches, including the two-equation model of Liu *et al.*,[3] are able to predict the order of magnitude of the primary particle number density.

Figure 10 shows the soot volume fraction, mean primary particle diameter, mean primary particle number, and aggregate number density on the flame centerline along with the experimental data of Santoro *et al.*[42] and

Downloaded by Clinton Groth on January 1, 2022 | http://arc.aiaa.org | DOI: 10.2514/6.2022-2253

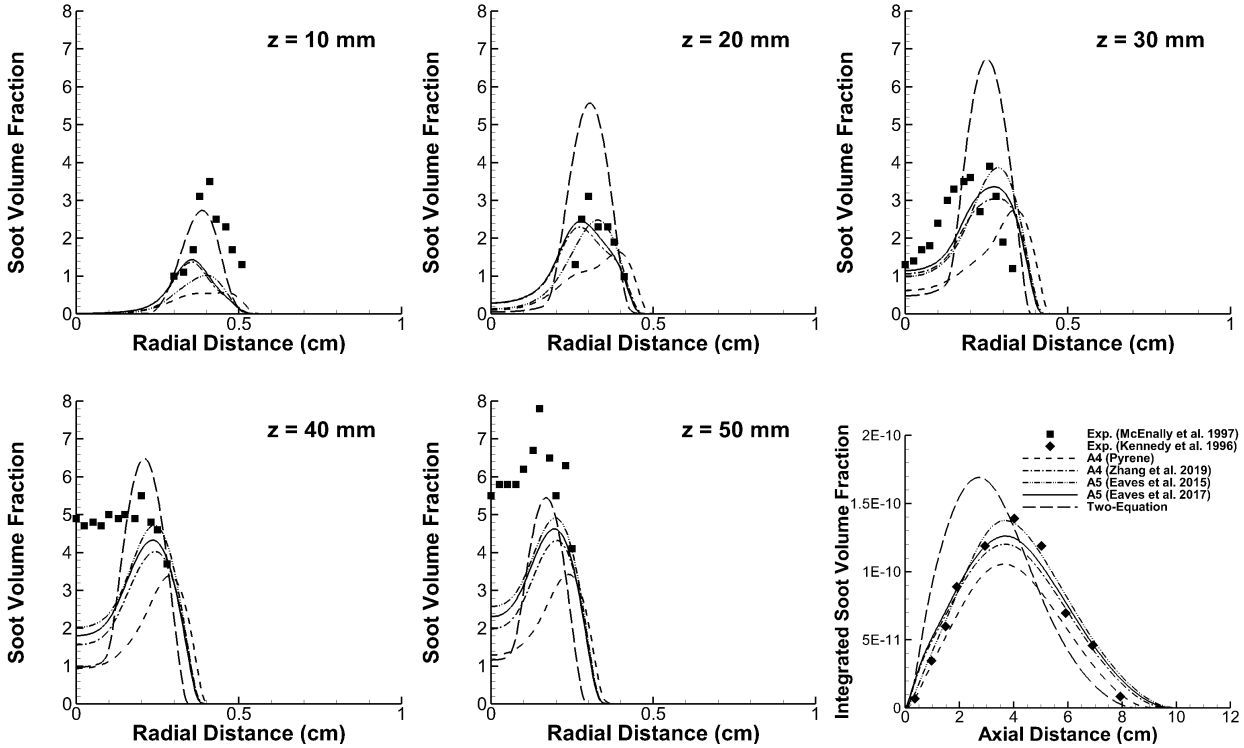

Figure 8. Radial and radially integrated soot volume fraction profiles for the Santoro laminar diffusion flame. Experimental data from McEnally *et al.*[81] and Kennedy *et al.*[80]

of Koylu *et al.*[82] Results indicate that the 5-ring model of Eaves *et al.* (2015)[44] predicts well the centerline soot volume fraction while the pyrene model presents an underprediction of more than a factor 2. The centerline mean primary particle diameter is relatively well predicted by all PAH-based approaches except for the pyrene model. However, all PAH models show a downstream shift of the primary particle diameter profile comparatively to experimental data. In comparison, while the two-equation model of Liu *et al.*[3] predicts well the primary particle diameter, the centerline soot volume fraction is significantly underpredicted. Figure 10 indicates a significant underprediction of the mean primary particle number for all PAH models. This underprediction can be due to uncertainity of the soot sintering rate and coagulation efficiency. Notably, the introduction of size-dependent coagulation efficiency[108–112] could improve numerical results. However, the exploration of size-dependent coagulation efficiency will be left for future work. Additionally, Figure 10 indicates that the plateau of aggregate number density is well predicted with all PAH models except for pyrene. Additionally, results indicate that all PAH models present a downstream shift of about 2.0 cm of the aggregate number density profile. Again, the two-equation model of Liu *et al.*[3] does not consider aggregation and predicts neither the evolution of the mean primary particle number nor the aggregate number density. Finally, some of the discrepancies observed on the centerline could be reduced by using CHT. However, such work is left for future studies.

IV.A.3. Effects of Sintering Rate on Soot Formation

Uncertainities of the sintering rate was suggested to explain some of the discrepancies observed in the numerical results presented above. Notably, the application of sintering to soot prediction is still relatively new and the rate of sintering is not well understood. In this respect, results obtained without sintering, with the sintering model of Veshkini *et al.*,[69] with the sintering model of Chen *et al.*,[113] and with a pure coalescence model are compared below on Figure 11 for the maximum sootline and on Figure 12 for the centerline. All simulations here are obtained with the 5-ring PAH model of Eaves *et al.* (2015).[44] Overall, results show some improvements of the prediction of the primary number density with the sintering model of Chen *et al.*[113] However, the same model also lead to an important underprediction of mean primary particle diameter. On the other hand, results without sintering show an important overprediction of mean primary

Downloaded by Clinton Groth on January 1, 2022 | http://arc.aiaa.org | DOI: 10.2514/6.2022-2253

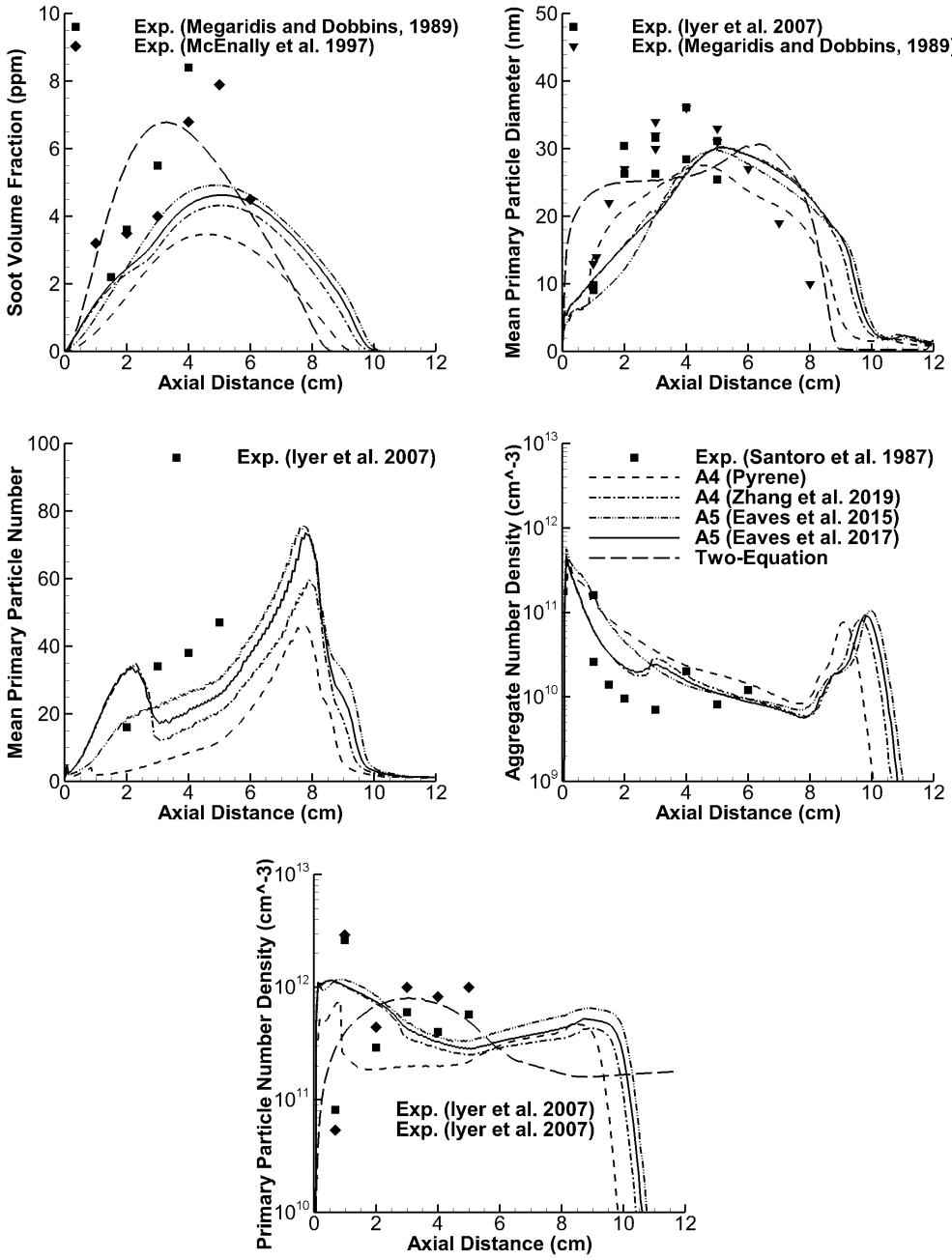

Figure 9. Comparison of soot volume fraction, mean primary particle diameter, mean primary particle number, aggregate number density, and primary particle number density along the maximum sootline for the Santoro laminar diffusion flame. Experimental data from Santoro *et al.*,[76] Megaridis and Dobbins,[78] McEnally *et al.*,[81] and from Iyer *et al.*[83]

particle number on both the maximum sootline and the centerline with a significant underprediction of the mean primary particle diameter. Additionally, neglecting sintering results in an overestimation of primary particle density number on the line of maximum soot concentration. Results hence indicate that sintering play an important role in the prediction of the evolution of the morphology of soot particles. Finally, results with pure coalescence, which corresponds to an univariate model since all particles are assumed to be spherical, show poor predictions of aggregate number density and/or primary particle density number on both the centerline and the line of maximum soot concentration. In addition, the pure coalescence model results in an underprediction of soot volume fraction on the line of maximum soot concentration. Hence, the results above show the importance of a finite rate coalescence (or sintering) in the accurate prediction of

Downloaded by Clinton Groth on January 1, 2022 | http://arc.aiaa.org | DOI: 10.2514/6.2022-2253

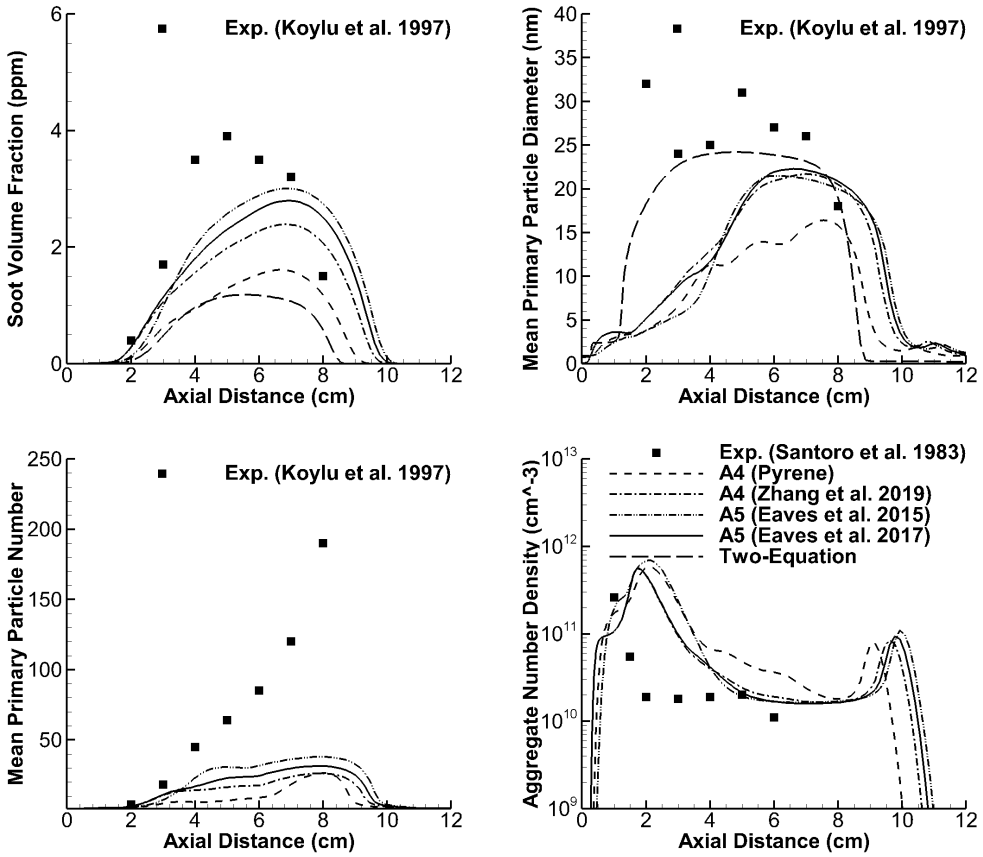

Figure 10. Comparison of soot volume fraction, mean primary particle diameter, mean primary particle number, and aggregate number density along the centerline for the Santoro laminar diffusion flame. Experimental data from Santoro *et al.*[42] and from Koylu *et al.*[82]

soot morphology. However, no clear superiority of one sintering model can be demonstrated. Consequently, additional study of the sintering rate is necessary in order to improve the prediction of soot morphology. Alternatively, a multi-regime coagulation model as suggested by Mueller *et al.*[14] can also be considered. However, the further study of coagulation, coalescence, and/or sintering of soot particles will be left for future work.

IV.A.4. Effects of Coagulation Efficiency on Soot Formation

In order to study the effects of coagulation efficiency on soot morphology, coagulation efficiencies of 0.2, 0.5, 0.8, and 1 are considered herein along with the 5-ring PAH model of Eaves *et al.* (2015).[44] Figure 13 shows that soot volume fraction is not sensitive to the coagulation efficiency. However, the mean number of primary particle per aggregate and the aggregate number density are significantly impacted by an increase of the coagulation efficiency. Results indicate that increasing the coagulation efficiency above 0.2 leads to a premature growth of primary particle number and to an underprediction of the aggregate number density. Consequently, results obtained here confirm previous numerical studies that a coagulation efficiency of 0.2 reproduces well the morphology of soot particles in the Santoro burner.[8,69,85,86]

IV.A.5. Effects of Fragmentation Rate on Soot Formation

Oxidation-induced fragmentation can also affect the soot morphology. In this respect, in order to investigate the sensitivity of the fragmentation rate on the prediction of soot morphology, numerical simulations are also realized with the fragmentation model of Sirignano *et al.*[114] and without fragmentation. All simulations here are obtained with the 5-ring PAH model of Eaves *et al.* (2015).[44] Results on Figure 14 indicate that, as expected, fragmentation does not affect the prediction of soot volume fraction. On the other hand, it

Downloaded by Clinton Groth on January 1, 2022 | http://arc.aiaa.org | DOI: 10.2514/6.2022-2253

Downloaded by Clinton Groth on January 1, 2022 | http://arc.aiaa.org | DOI: 10.2514/6.2022-2253

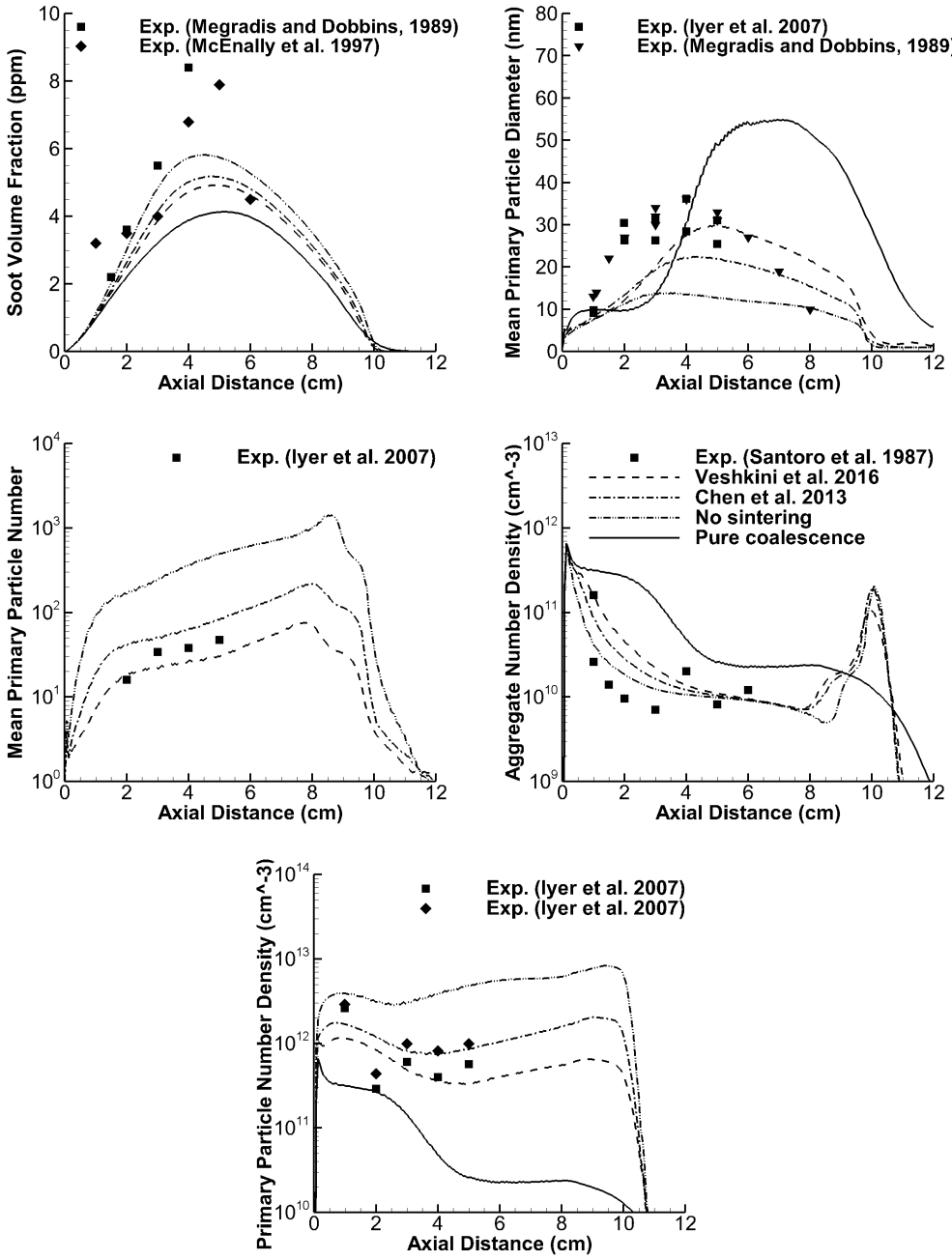

Figure 11. Comparison of soot volume fraction, mean primary particle diameter, mean primary particle number, aggregate number density, and primary particle number density along the maximum sootline for the Santoro laminar diffusion flame for different sintering models. Experimental data from Santoro *et al.*,[76] Megaridis and Dobbins,[78] McEnally *et al.*,[81] and from Iyer *et al.*[83]

can be seen that around ~ 7 cm above the burner, when oxidation dominate over condensation and surface growth, the size of aggregates in terms of number of primary particles starts to decrease. This reduction of mean primary particles number per aggregate is due to the fragmentation of larger aggregates into smaller ones, a process that preserve both the total volume and the total number of primary particles, but results in an increase of aggregate density number. In addition, results indicate that the fragmentation models of Sirignano *et al.*[114] and of Mueller *et al.*[70] give very similar predictions of the rate of fragmentation for this flame. Notably, both models lead to a similar increase of aggregate number density at the downstream end of the flame. However, the lack of experimental data above ~ 8 cm the burner prevents the further validation of fragmentation models in laminar coflow diffusion flames.

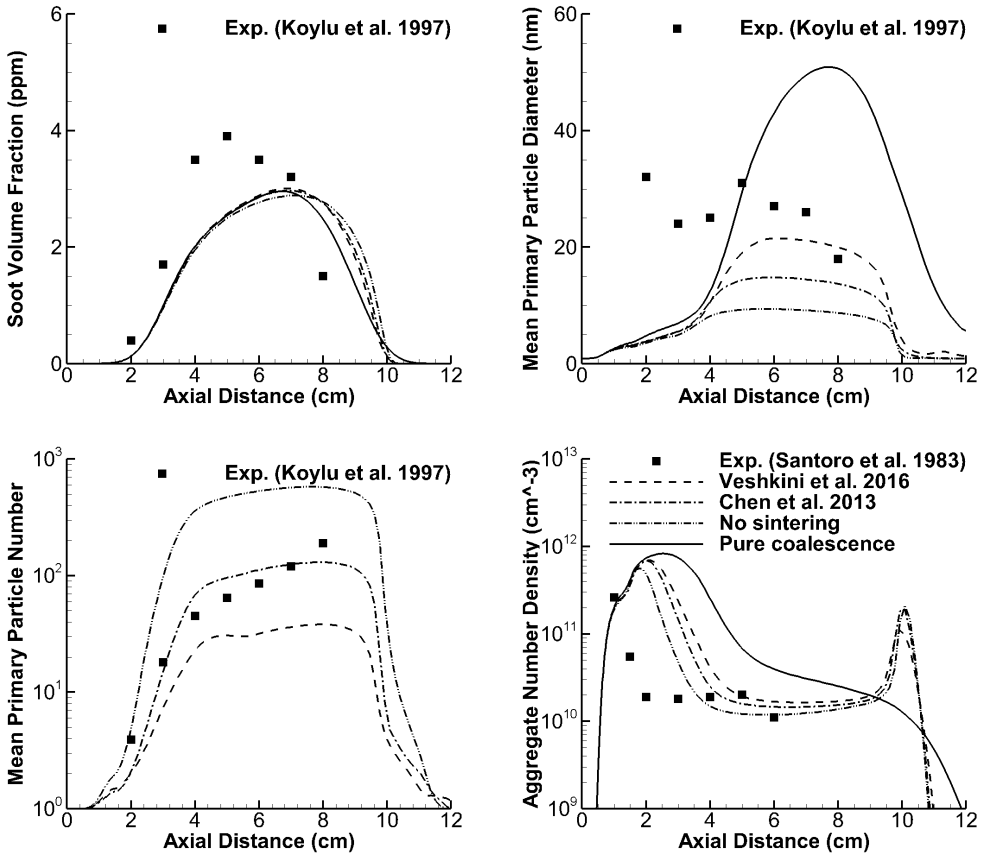

Figure 12. Comparison of soot volume fraction, mean primary particle diameter, mean primary particle number, and aggregate number density along the centerline for the Santoro laminar diffusion flame for different sintering models. Experimental data from Santoro *et al.*[42] and from Koylu *et al.*[82]

IV.B. Smooke-Long Burner Laminar Co-Flow Diffusion Flames

Consider next the results for the Smooke-Long burner. Figure 15 compares the predicted centerline temperature with the experimental data of Smooke *et al.*[91] and of Satija *et al.*[103] Results indicate reasonably well predicted centerline temperature profiles. However, it can be noticed that generally the numerical centerline temperature profiles are further shifted downstream comparatively to experimental data. A similar shift can be observed in the numerical results of Smooke *et al.*,[91] Veshkini *et al.*,[7] or Botero *et al.*[104] However, discrepancies in experimental temperature can also be observed between the measurements of Smooke *et al.*[91] of Satija *et al.*[103] with the latter in better agreement with the current numerical results. Additionally, numerical results show that the predicted flames are longer than the experimental flames. However, such behavior has been commonly observed in previous numerical studies.[7,91,104]

Figure 16 compares the predicted soot volume fraction with the experimental data of Smooke *et al.*[10] Results show notably that PAH-based seven-moment CQMOM-Radau results do not predict well the soot volume fraction at lower ethylene concentrations (32% and 40%). The experimental data indicate that the wing structure disappears at lower ethylene concentrations and that the peak location of soot volume fraction shift to the centerline. In contrast, the numerical results indicate that the wing structure is still present at lower ethylene concentrations. However, similar behaviors have been reported previously by Smooke *et al.*,[91] Khosousi and Dworkin,[107] and Veshkini *et al.*[7] from sectional results. The discrepancies between numerical simulations and experimental data suggest uncertainities in PAH inception and condensation models at high dilution level. Neverthless, numerical results here indicate that reasonable prediction of the peak soot volume fraction can be obtained with the values of the steric factor used herein. Regarding the two-equation model of Liu *et al.*,[3] numerical results indicate reasonable prediction of peak soot concentration in the wings with an underprediction on the centerline which results in an overprediction of centerline temperature. Overall, a better agreement of the peak soot volume fraction could be obtained by a more careful calibration of the

Downloaded by Clinton Groth on January 1, 2022 | http://arc.aiaa.org | DOI: 10.2514/6.2022-2253

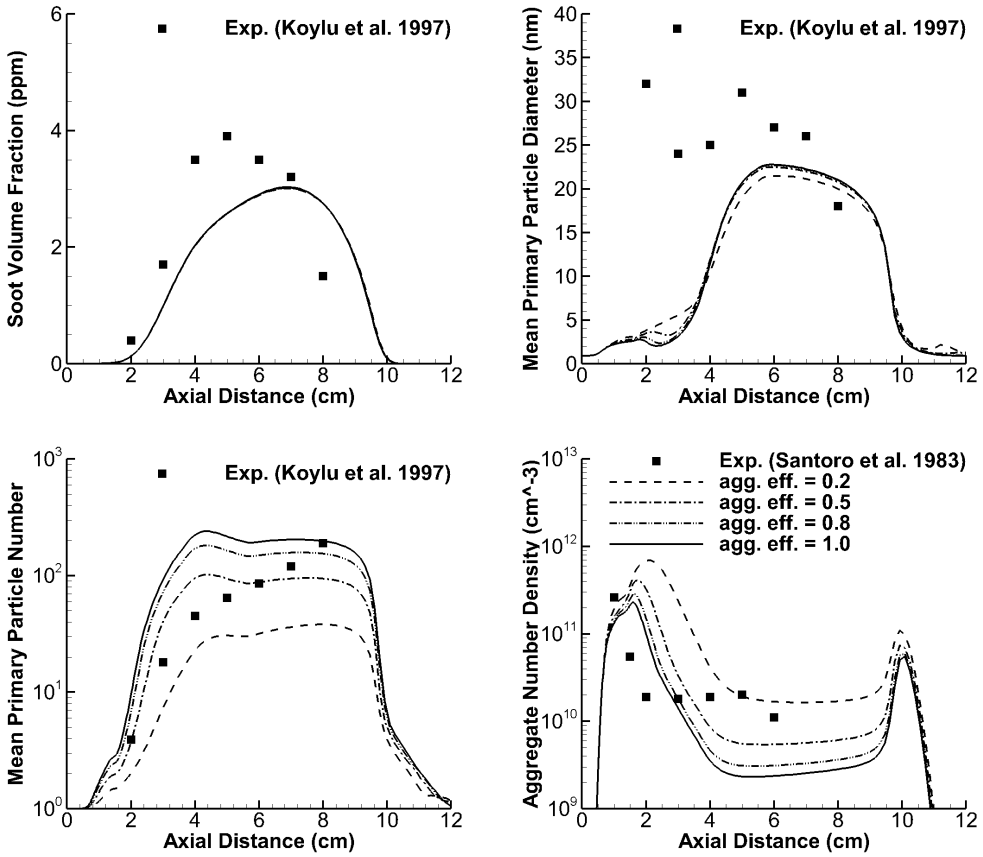

Figure 13. Comparison of soot volume fraction, mean primary particle diameter, mean primary particle number, and aggregate number density along the centerline for the Santoro laminar diffusion flame for different aggregation efficiencies. Experimental data from Santoro *et al.*[42] and from Koylu *et al.*[82]

steric factor for each dilution level and for each precursor models. However, such approach is not adopted here since the primary focus is on the effects of PAHs precursors on soot formation and not on the study of the steric factor. In this respect, results indicate that the inclusion of smaller PAH species (models of Zhang *et al.*[57] and of Eaves *et al.* (2017)[45]) results in an early and premature inception of soot. Similar behaviors have been observed by Zhang *et al.*[57] in methane doped flames. Finally, although the pyrene-based model underpredicts the peak soot concentration, this model seems to better reproduce the soot concentration qualitatively for the Smooke-Long burner.

Finally, Figure 17 compares the gyration radius obtained with PAH-based models with the experimental data of Kempema *et al.*[102] for the case with 60% and 80% ethylene. Since the two-equation model of Liu *et al.*[3] only predicts primary particle diameter, results from this model are not indicated here. Results indicate a consistent underprediction of the gyration radius for all PAH precursors. The lower gyration radius obtained numerically can be explained by an under estimation of the diameter of each primary particle, an underestimation of the number of primary particles per aggregate or a combination of both. The discrepancies can be explained by uncertainity in the sintering model used in the numerical simulations since the inclusion of soot sintering in numerical simulations is still relatively new. In addition, the adoption of a size-dependent aggregation efficiency could also led to improved results. However, such studies will be left for future work.

V. Conclusions

The present investigation of the effects of various PAH precursors on the predicted soot formation in the laminar co-flow diffusion flames of the Santoro and Smooke-Long burners using the recently proposed seven-moment fractional-order CQMOM-Radau moment closure of Xing *et al.*[41] indicate that the seven-

Downloaded by Clinton Groth on January 1, 2022 | http://arc.aiaa.org | DOI: 10.2514/6.2022-2253

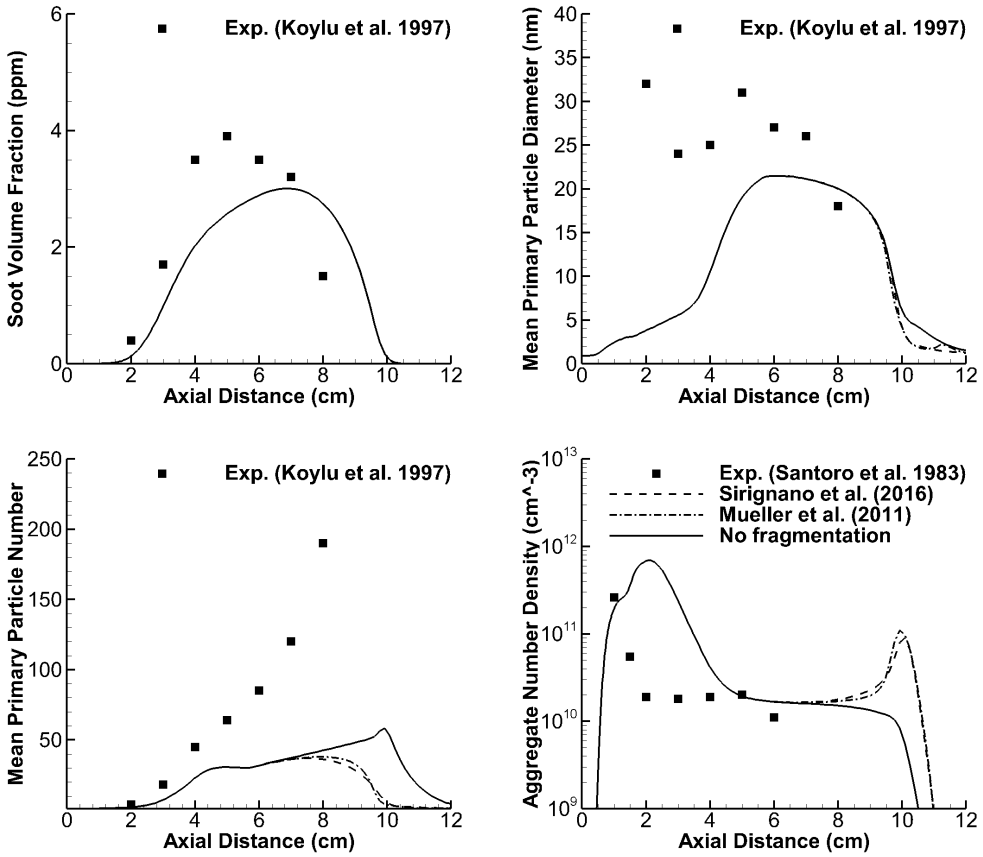

Figure 14. Comparison of soot volume fraction, mean primary particle diameter, mean primary particle number, and aggregate number density along the centerline for the Santoro laminar diffusion flame for different fragmentation models. Experimental data from Santoro *et al.*[42] and from Koylu *et al.*[82]

moment description is capable of representing the fractal structure of the soot aggregrates and allowing a treatment for PAH-based nucleation. The results of the study also indicate that the predicted levels of soot formation are sensitive to the choice of PAH species. The simulation results also suggest that the inclusion of PAH species smaller than the 4-ring pyrene leads to an early and premature formation of soot particles. Conversely, while the inclusion of larger, 5-ring PAHs, can lead to some improvements of soot predictions, no absolute advantage of 5-ring PAHs has been shown. Finally, if one is not interested in the morphology of soot particles, it would seem that a "well-tuned" semi-empirical two-equation model can predict reasonably well the soot volume fraction, albeit with an underprediction of the soot concentration along the centerline of the diffusion flames.

Acknowledgements

This research was funded by grants and contracts from the Green Aviation Research and Development Network (GARDN), Southern Ontario Smart Computing for Innovation Platform (SOSCIP), as well as Pratt & Whitney Canada. The first author also received support in the form of a scholarship from the Natural Sciences and Engineering Research Council (NSERC) of Canada. Additionally, the computational resources for performing the numerical simulations reported herein were provided by the SOSCIP program as well as the SciNet High Performance Computing Consortium at the University of Toronto and Compute/Calcul Canada (the latter are funded by the Canada Foundation for Innovation (CFI) and Province of Ontario, Canada).

Downloaded by Clinton Groth on January 1, 2022 | http://arc.aiaa.org | DOI: 10.2514/6.2022-2253

Downloaded by Clinton Groth on January 1, 2022 | http://arc.aiaa.org | DOI: 10.2514/6.2022-2253

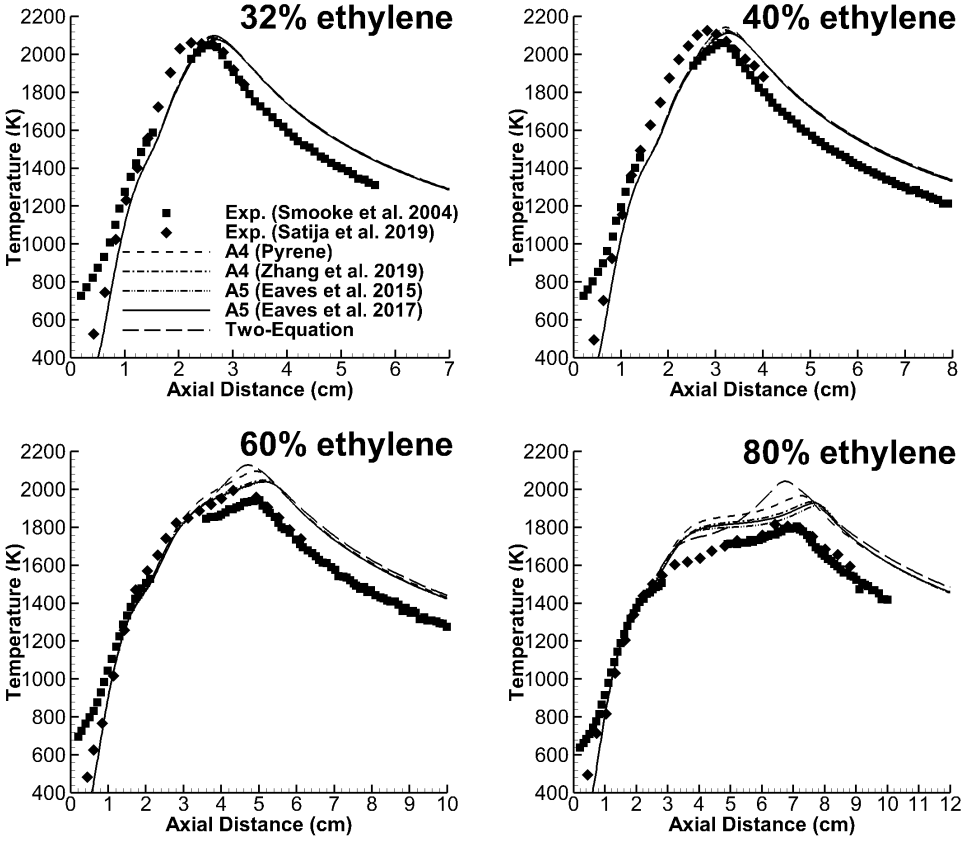

Figure 15. Centerline temperature profiles for the Smooke laminar diffusion flame. Experimental data from Smooke *et al.*[91] and Satija *et al.*[103]

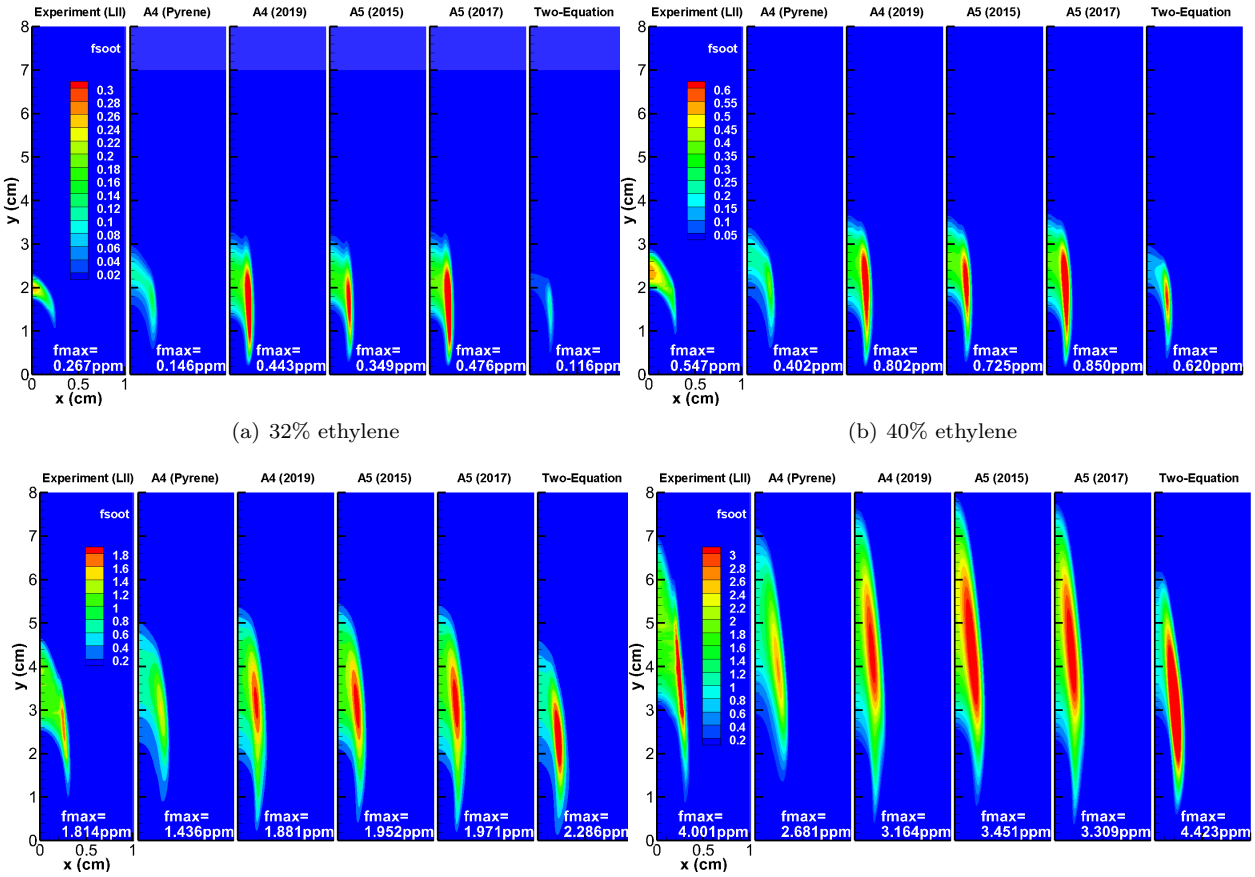

(a) 32% ethylene (b) 40% ethylene

(c) 60% ethylene (d) 80% ethylene

Figure 16. Soot volume fraction isopleth for the Smooke laminar diffusion flame. Experimental data from Smooke *et al.*[10]

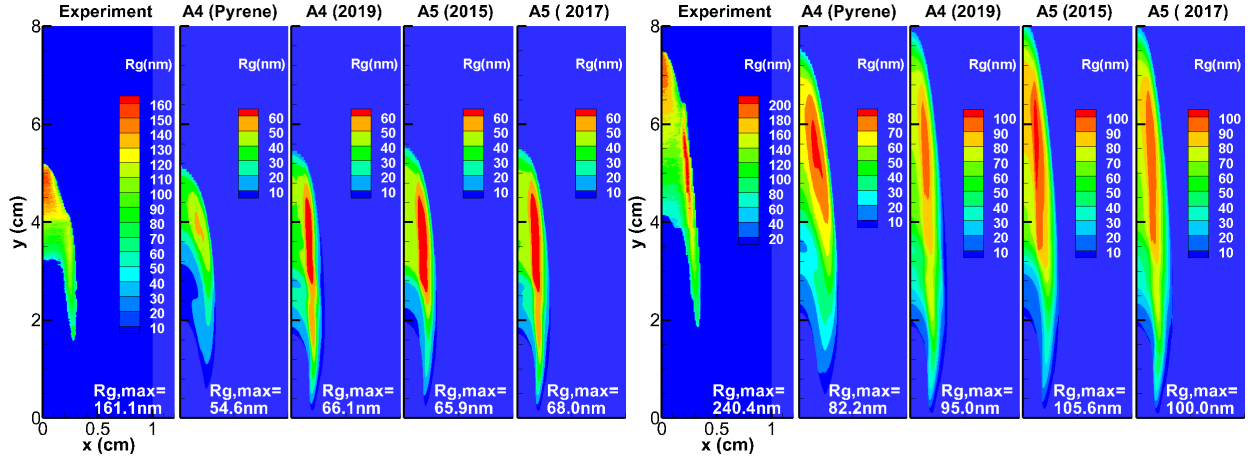

(a) 60% ethylene (b) 80% ethylene

Figure 17. Gyration radius isopleth for the Smooke laminar diffusion flame. Experimental data from Kempema *et al.*[102]

Downloaded by Clinton Groth on January 1, 2022 | http://arc.aiaa.org | DOI: 10.2514/6.2022-2253

References

[1]Leung, K. M., Lindstedt, R. P., and Jones, W. P., "A simplified reaction mechanism for soot formation in nonpremixed flames," *Combustion and Flame*, Vol. 87, No. 3-4, 1991, pp. 289–305.

[2]Fairweather, M., Jones, W. P., and Lindstedt, R. P., "Predictions of radiative transfer from a turbulent reacting jet in a cross-wind," *Combustion and Flame*, Vol. 89, No. 1, 1992, pp. 45–63.

[3]Liu, F., Guo, H., Smallwood, G. J., and Gulder, O. L., "Effects of gas and soot radiation on soot formation in a coflow laminar ethylene diffusion flame," *Journal of Quantitative Spectroscopy and Radiative Transfer*, Vol. 73, No. 2-5, 2002, pp. 409–421.

[4]Jerez, A., Villanueva, J. C., da Silva, L. F., Demarco, R., and Fuentes, A., "Measurements and modeling of PAH soot precursors in coflow ethylene/air laminar diffusion flames," *Fuel*, Vol. 236, 2019, pp. 452–460.

[5]Frenklach, M. and Wang, H., "Detailed modeling of soot particle nucleation and growth," *Twenty-Third Symposium (International) on Combustion*, 1991, pp. 1559–1566.

[6]Zhang, Q., Guo, H., Liu, F., Smallwood, G. J., and Thompson, M. J., "Modeling of soot aggregate formation and size distribution in a laminar ethylene/air coflow diffusion flame with detailed PAH chemistry and an advanced sectional aerosol dynamics model," *Proceedings of the Combustion Institute*, Vol. 32, 2009, pp. 761–768.

[7]Veshkini, A., Dworkin, S. B., and Thomson, M. J., "A soot particle surface reactivity model applied to a wide range of laminar ethylene/air flames," *Combustion and Flame*, Vol. 161, No. 12, 2014, pp. 3191–3200.

[8]Eaves, N. A., Zhang, Q., Liu, F., Guo, H., Dworkin, S. B., and Thomson, M. J., "CoFlame: A refined and validated numerical algorithm for modeling sooting laminar coflow diffusion flames," *Computer Physics Communications*, Vol. 207, 2016, pp. 464–477.

[9]Wang, Y., Raj, A., and Chung, S. H., "Soot modeling of counterflow diffusion flames of ethylene-based binary mixture fuels," *Combustion and Flame*, Vol. 162, No. 3, 2015, pp. 586–596.

[10]Smooke, M. D., Long, M. B., Connelly, B. C., Colket, M. B., and Hall, R. J., "Soot formation in laminar diffusion flames," *Combustion and Flame*, Vol. 143, No. 4, 2005, pp. 613–628.

[11]D'Anna, A. and Kent, J. H., "Modeling of particulate carbon and species formation in coflowing diffusion flames of ethylene," *Combustion and Flame*, Vol. 144, No. 1-2, 2006, pp. 249–260.

[12]Zhang, Q., Guo, H., Liu, F., Smallwood, G. J., and Thompson, M. J., "Implementation of an advanced fixed sectional aerosol dynamics model with soot aggregate formation in a laminar methane/air coflow diffusion flame," *Combustion Theory and Modelling*, Vol. 12, No. 4, 2008, pp. 621–641.

[13]Frenklach, M., "Method of moments with interpolative closure," *Chemical Engineering Science*, Vol. 57, No. 12, 2002, pp. 2229–2239.

[14]Mueller, M. E., Blanquart, G., and Pitsch, H., "Hybrid method of moments for modeling soot formation and growth," *Combustion and Flame*, Vol. 156, No. 6, 2009, pp. 1143–1155.

[15]McGraw, R., "Description of Aerosol Dynamics by the Quadrature Method of Moments," *Aerosol Science and Technology*, Vol. 27, No. 2, 1997, pp. 255–265.

[16]Sung, Y., Raman, V., Koo, H., Mehta, M., and Fox, R. O., "Large eddy simulation modeling of turbulent flame synthesis of titania nanoparticles using a bivariate particle description," *AIChE Journal*, Vol. 60, No. 2, 2014, pp. 459–472.

[17]Salenbauch, S., Cuoci, A., Frassoldati, A., Saggese, C., Faravelli, T., and Hasse, C., "Modeling soot formation in premixed flames using an Extended Conditional Quadrature Method of Moments," *Combustion and Flame*, Vol. 162, No. 6, 2015, pp. 2529–2543.

[18]Wick, A., Nguyen, I. T.-T., Laurent, F., Fox, R. O., and Pitsch, H., "Modeling soot oxidation with the Extended Quadrature Method of Moments," *Proceedings of the Combustion Institute*, Vol. 36, 2017, pp. 789–797.

[19]Marchisio, D. L., Pikturna, J. T., Fox, R. O., Vigil, R. D., and Barresi, A. A., "Quadrature method of moments for population-balance equations," *AIChE Journal*, Vol. 49, No. 5, 2003, pp. 1266–1276.

[20]Marchisio, D. L., Vigil, R. D., and Fox, R. O., "Quadrature method of moments for aggregation-breakage processes," *Journal of Colloid and Interface Science*, Vol. 258, No. 2, 2003, pp. 322–334.

[21]Marchisio, D. L., Vigil, R. D., and Fox, R. O., "Implementation of the quadrature method of moments in CFD codes for aggregation-breakage problems," *Journal of Colloid and Interface Science*, Vol. 58, No. 15, 2003, pp. 3337–3351.

[22]Wright, D. L., McGraw, R., and Rosner, D. E., "Bivariate extension of the quadrature method of moments for modeling simultaneous coagulation and sintering of particle populations," *Journal of Colloid and Interface Science*, Vol. 236, No. 2, 2001, pp. 242–251.

[23]Gordon, R. G., "Error bounds in equilibrium statistical mechanics," *Journal of Mathematical Physics*, Vol. 9, No. 5, 1968, pp. 655–663.

[24]Wheeler, J. C., "Modified moments and Gaussian quadratures," *Rocky Mountain Journal of Mathematics*, Vol. 4, No. 2, 1974, pp. 287–296.

[25]Fan, R., Marchisio, D. L., and Fox, R. O., "Application of the direct quadrature method of moments to polydisperse gas-solid fluidized beds," *Powder Technology*, Vol. 139, No. 1, 2004, pp. 7–20.

[26]Marchisio, D. L. and Fox, R. O., "Solution of population balance equations using the direct quadrature method of moments," *Journal of Aerosol Science*, Vol. 36, No. 1, 2005, pp. 43–73.

[27]Fox, R. O., "Bivariate direct quadrature method of moments for coagulation and sintering of particle populations," *Journal of Aerosol Science*, Vol. 37, No. 11, 2006, pp. 1562–1580.

[28]Zucca, A., Marchisio, D. L., Vanni, M., and Barresi, A. A., "Validation of bivariate DQMOM for nanoparticle processes simulation," *AIChE Journal*, Vol. 53, No. 4, 2007, pp. 918–931.

Downloaded by Clinton Groth on January 1, 2022 | http://arc.aiaa.org | DOI: 10.2514/6.2022-2253

[29]Buffo, A., Vanni, M., and Marchisio, D. L., "Multidimensional population balance model for the simulation of turbulent gas-liquid systems in stirred tank reactors," *Chemical engineering science*, Vol. 70, 2012, pp. 31–44.

[30]Zucca, A., Marchisio, D. L., Barresi, A. A., and Fox, R. O., "Implementation of the population balance equation in CFD codes for modelling soot formation in turbulent flames," *Chemical Engineering Science*, Vol. 61, No. 1, 2006, pp. 87–95.

[31]Marchisio, D. L. and Barresi, A. A., "Investigation of soot formation in turbulent flames with a pseudo-bivariate population balance model," *Chemical Engineering Science*, Vol. 64, No. 2, 2009, pp. 294–303.

[32]Blanquart, G. and Pitsch, H., "A joint volume-surface-hydrogen multi-variate model for soot formation," *Combustion generated fine carbonaceous particles*, 2009, pp. 437–463.

[33]Blanquart, G. and Pitsch, H., "Analyzing the effects of temperature on soot formation with a joint volume-surface-hydrogen model," *Combustion and Flame*, Vol. 156, No. 8, 2009, pp. 1614–1626.

[34]Chan, T. L., Liu, Y. H., and Chan, C. K., "Direct quadrature method of moments for the exhaust particle formation and evolution in the wake of the studied ground vehicle," *Journal of Aerosol Science*, Vol. 41, No. 6, 2010, pp. 553–568.

[35]Chittipotula, T., Janiga, G., and Thévenin, D., "Improved soot prediction models for turbulent non-premixed ethylene/air flames," *Proceedings of the Combustion Institute*, Vol. 33, No. 1, 2011, pp. 559–567.

[36]Kim, T. and Kim, Y., "DQMOM approach for poly-dispersed soot formation processes in a turbulent non-premixed ethylene/air flame," *Chemical Engineering Science*, Vol. 152, 2016, pp. 426–435.

[37]Buffo, A., Vanni, M., Marchisio, D. L., and Fox, R. O., "Multivariate quadrature-based moments methods for turbulent polydisperse gas–liquid systems," *International Journal of Multiphase Flow*, Vol. 50, 2013, pp. 41–57.

[38]Yuan, C. and Fox, R. O., "Conditional quadrature method of moments for kinetic equations," *Journal of Computational Physics*, Vol. 230, No. 22, 2011, pp. 8216–8246.

[39]Buffo, A., Marchisio, D. L., Vanni, M., and Renze, P., "Simulation of polydisperse multiphase systems using population balances and example application to bubbly flows," *Chemical Engineering Research and Design*, Vol. 91, No. 10, 2013, pp. 1859–1875.

[40]Petitti, M., Vanni, M., Marchisio, D. L., Buffo, A., and Podenzani, F., "Simulation of coalescence, break-up and mass transfer in a gas–liquid stirred tank with CQMOM," *Chemical Engineering Journal*, Vol. 228, 2013, pp. 1182–1194.

[41]Xing, J. Y., Groth, C. P. T., and Hu, J. T. C., "On the Use of Fractional-Order Quadrature-Based Moment Closures for Predicting Soot Formation in Laminar Flames," *Combustion Science and Technology*, 2019, pp. 1–23.

[42]Santoro, R. J., Semerjian, H. G., and Dobbins, R. A., "Soot particle measurements in diffusion flames," *Combustion and Flame*, Vol. 51, 1983, pp. 203–218.

[43]Slavinskaya, N. A., Riedel, U., Dworkin, S. B., and Thomson, M. J., "Detailed numerical modeling of PAH formation and growth in non-premixed ethylene and ethane flames," *Combustion and Flame*, Vol. 159, No. 3, 2012, pp. 979–995.

[44]Eaves, N. A., Dworkin, S. B., and Thomson, M. J., "The importance of reversibility in modeling soot nucleation and condensation processes," *Proceedings of the Combustion Institute*, Vol. 35, No. 2, 2015, pp. 1787–1794.

[45]Eaves, N. A., Dworkin, S. B., and Thomson, M. J., "Assessing relative contributions of PAHs to soot mass by reversible heterogeneous nucleation and condensation," *Proceedings of the Combustion Institute*, Vol. 36, No. 1, 2017, pp. 935–945.

[46]Fairweather, M., Jones, W. P., Ledin, H. S., and Lindstedt, R. P., "Predictions of soot formation in turbulent, non-premixed propane flames," *Twenty-Fourth Symposium on Combustion*, The Combustion Institute, 1992, pp. 1067–1074.

[47]Ezekoye, O. A. and Zhang, Z., "Soot oxidation and agglomeration modeling in a microgravity diffusion flame," *Combustion and Flame*, Vol. 110, No. 1-2, 1997, pp. 127–139.

[48]Kronenburg, A., Bilger, R. W., and Kent, J. H., "Modeling soot formation in turbulent methane-air jet diffusion flames," *Combustion and Flame*, Vol. 121, No. 1-2, 2000, pp. 24–40.

[49]Guo, H., Liu, F., Smallwood, G. J., and Gulder, O. L., "The flame preheating effect on numerical modelling of soot formation in a two-dimensional laminar ethylene-air diffusion flame," *Combustion Theory and Modelling*, Vol. 6, 2002, pp. 173–188.

[50]Liu, F., Guo, H., Smallwood, G. J., and Gulder, O. L., "Numerical modelling of soot formation and oxidation in laminar coflow non-smoking and smoking ethylene diffusion flames," *Combustion Theory and Modelling*, Vol. 7, No. 2, 2003, pp. 301–315.

[51]Liu, F., Thomson, K. A., Guo, H., and Smallwood, G. J., "Numerical and experimental study of an axisymmetric coflow laminar methane-air diffusion flame at pressures between 5 and 40 atmospheres," *Combustion and Flame*, Vol. 146, No. 3, 2006, pp. 456–471.

[52]Dworkin, S. B., Zhang, Q., Thomson, M. J., Slavinskaya, N. A., and Riedel, U., "Application of an enhanced PAH growth model to soot formation in a laminar coflow ethylene/air diffusion flame," *Combustion and Flame*, Vol. 158, No. 9, 2011, pp. 1682–1695.

[53]Vishwanathan, G. and Reitz, R. D., "Development of a practical soot modeling approach and its application to low-temperature diesel combustion," *Combustion Science and Technology*, Vol. 182, No. 8, 2010, pp. 1050–1082.

[54]Vishwanathan, G. and Reitz, R. D., "Application of a semi-detailed soot modeling approach for conventional and low temperature diesel combustion - Part I: Model performance," *Fuel*, Vol. 139, 2015, pp. 757–770.

[55]Consalvi, J.-L., Liu, F., Contreras, J., Kashif, M., Legros, G., Shuai, S., and Wang, J., "Numerical study of soot formation in laminar coflow diffusion flames of methane doped with primary reference fuels," *Combustion and flame*, Vol. 162, No. 4, 2015, pp. 1153–1163.

[56]Consalvi, J.-L., Liu, F., Kashif, M., and Legros, G., "Numerical study of soot formation in laminar coflow methane/air diffusion flames doped by n-heptane/toluene and iso-octane/toluene blends," *Combustion and Flame*, Vol. 180, 2017, pp. 167–174.

[57]Zhang, C., Chen, L., Ding, S., Xu, H., Li, G., Consalvi, J.-L., and Liu, F., "Effects of soot inception and condensation PAH species and fuel preheating on soot formation modeling in laminar coflow CH4/air diffusion flames doped with n-heptane/toluene mixtures," *Fuel*, Vol. 253, 2019, pp. 1371–1377.

Downloaded by Clinton Groth on January 1, 2022 | http://arc.aiaa.org | DOI: 10.2514/6.2022-2253

[58]Raj, A., Sander, M., Janardhanan, V., and Kraft, M., "A study on the coagulation of polycyclic aromatic hydrocarbon clusters to determine their collision efficiency," *Combustion and Flame*, Vol. 157, No. 3, 2010, pp. 523–534.

[59]Di Domenico, M., Gerlinger, P., and Aigner, M., "Development and validation of a new soot formation model for gas turbine combustor simulations," *Combustion and Flame*, Vol. 157, No. 2, 2010, pp. 246–258.

[60]Blacha, T., Domenico, M. D., Gerlinger, P., and Aigner, M., "Soot predictions in premixed and non-premixed laminar flames using a sectional approach for PAHs and soot," *Combustion and Flame*, Vol. 159, No. 1, 2012, pp. 181–193.

[61]Eberle, C., Gerlinger, P., and Aigner, M., "A sectional PAH model with reversible PAH chemistry for CFD soot simulations," *Combustion and Flame*, Vol. 179, 2017, pp. 63–73.

[62]Rogak, S. N. and Flagan, R. C., "Coagulation of aerosol agglomerates in the transition regime," *Journal of Colloid and Interface Science*, Vol. 151, No. 1, 1992, pp. 203–224.

[63]Zurita-Gotor, M. and Rosner, D. E., "Effective diameters for collisions of fractal-like aggregates: Recommendations for improved aerosol coagulation frequency predictions," *Journal of colloid and interface science*, Vol. 255, No. 1, 2002, pp. 10–26.

[64]Naumann, K.-H., "COSIMA—a computer program simulating the dynamics of fractal aerosols," *Journal of Aerosol Science*, Vol. 34, No. 10, 2003, pp. 1371–1397.

[65]Phillips, W. F., "Drag on a small sphere moving through a gas," *The Physics of Fluids*, Vol. 18, No. 9, 1975, pp. 1089–1093.

[66]Kazakov, A., Wang, H., and Frenklach, M., "Detailed modeling of soot formation in laminar premixed ethylene flames at a pressure of 10 bar," *Combustion and Flame*, Vol. 100, No. 1-2, 1995, pp. 111–120.

[67]Appel, J., Bockhorn, H., and Frenklach, M., "Kinetic modeling of soot formation with detailed chemistry and physics: laminar premixed flames of C2 hydrocarbons," *Combustion and Flame*, Vol. 121, No. 1-2, 2000, pp. 122–136.

[68]Park, S. H. and Rogak, S. N., "A one-dimensional model for coagulation, sintering, and surface growth of aerosol agglomerates," *Aerosol Science & Technology*, Vol. 37, No. 12, 2003, pp. 947–960.

[69]Veshkini, A., Dworkin, S. B., and Thomson, M. J., "Understanding soot particle size evolution in laminar ethylene/air diffusion flames using novel soot coalescence models," *Combustion Theory and Modelling*, Vol. 20, No. 4, 2016, pp. 707–734.

[70]Mueller, M. E., Blanquart, G., and Pitsch, H., "Modeling the oxidation-induced fragmentation of soot aggregates in laminar flames," *Proceedings of the Combustion Institute*, Vol. 33, 2011, pp. 667–674.

[71]Charest, M. R. J., *Numerical Modelling of Sooting Laminar Diffusion Flames at Elevated Pressures and Microgravity*, Ph.D. thesis, University of Toronto, 2010.

[72]Charest, M. R. J., Joo, H. I., Gulder, O. L., and Groth, C. P. T., "Experimental and numerical study of soot formation in laminar ethylene diffusion flames at elevated pressures from 10 to 35 atm," *Proceedings of the Combustion Institute*, Vol. 33, 2011, pp. 549–557.

[73]Charest, M. R. J., Groth, C. P. T., and Gülder, Ö. L., "A numerical study on the effects of pressure and gravity in laminar ethylene diffusion flames," *Combustion and Flame*, Vol. 158, No. 10, 2011, pp. 1933–1945.

[74]Charest, M. R. J., Gulder, O. L., and Groth, C. P. T., "Numerical and experimental study of soot formation in laminar diffusion flames burning simulated biogas fuels at elevated pressures," *Combustion and Flame*, Vol. 161, No. 10, 2014, pp. 2678–2691.

[75]"https://www.adelaide.edu.au/cet/isfworkshop/data-sets/laminar-flames," 2020, The University of Adelaide.

[76]Santoro, R. J., Yeh, T. T., Horvath, J. J., and Semerjian, H. G., "The transport and growth of soot particles in laminar diffusion flames," *Combustion Science and Technology*, Vol. 53, No. 2-3, 1987, pp. 89–115.

[77]Megaridis, C. M. and Dobbins, R. A., "Soot aerosol dynamics in a laminar ethylene diffusion flame," *Symposium (International) on Combustion*, Vol. 22, Elsevier, 1989, pp. 353–362.

[78]Megaridis, C. M. and Dobbins, R. A., "Comparison of soot growth and oxidation in smoking and non–smoking ethylene diffusion flames," *Combustion Science and Technology*, Vol. 66, No. 1-3, 1989, pp. 1–16.

[79]Puri, R. T., Richardson, T. F., Santoro, R. J., and Dobbins, R. A., "Aerosol dynamic processes of soot aggregates in a laminar ethene diffusion flame," *Combustion and flame*, Vol. 92, No. 3, 1993, pp. 320–333.

[80]Kennedy, I. M., Yam, C., Rapp, D. C., and Santoro, R. J., "Modeling and measurements of soot and species in a laminar diffusion flame," *Combustion and Flame*, Vol. 107, No. 4, 1996, pp. 368–382.

[81]McEnally, C. S., Köylü, Ü. Ö., Pfefferle, L. D., and Rosner, D. E., "Soot volume fraction and temperature measurements in laminar nonpremixed flames using thermocouples," *Combustion and Flame*, Vol. 109, No. 4, 1997, pp. 701–720.

[82]Köylü, Ü. Ö., McEnally, C. S., Rosner, D. E., and Pfefferle, L. D., "Simultaneous measurements of soot volume fraction and particle size/microstructure in flames using a thermophoretic sampling technique," *Combustion and Flame*, Vol. 110, No. 4, 1997, pp. 494–507.

[83]Iyer, S. S., Litzinger, T. A., Lee, S.-Y., and Santoro, R. J., "Determination of soot scattering coefficient from extinction and three-angle scattering in a laminar diffusion flame," *Combustion and flame*, Vol. 149, No. 1-2, 2007, pp. 206–216.

[84]Zhang, Q., *Detailed Modeling of Soot Formation/Oxidation in Laminar Coflow Diffusion Flame*, Ph.D. thesis, University of Toronto, 2009.

[85]Zhang, Q., Thomson, M. J., Guo, H., Liu, F., and Smallwood, G. J., "A numerical study of soot aggregate formation in a laminar coflow diffusion flame," *Combustion and Flame*, Vol. 156, No. 3, 2009, pp. 697–705.

[86]Veshkini, A., Eaves, N. A., Dworkin, S. B., and Thomson, M. J., "Application of PAH-condensation reversibility in modeling soot growth in laminar premixed and nonpremixed flames," *Combustion and Flame*, Vol. 167, 2016, pp. 335–352.

[87]Boedeker, L. R. and Dobbs, G. M., "Soot distribution and cars temperature measuremnts in axisymmetric laminar diffusion flames with several fuels," *Symposium (International) on Combustion*, Vol. 21, Elsevier, 1988, pp. 1097–1105.

[88]Thurgood, C. P., Pollard, A., and Becker, H. A., "The TN Quadrature Set for the Discrete Ordinates Method," *Journal of Heat Transfer*, Vol. 117, 1995, pp. 1069.

[89]Liu, F., Smallwood, G. J., and Gulder, O. L., "Application of the statistical narrow-band correlated-k method to low-resolution spectral intensity and radiative heat transfer calculations - effects of the quadrature scheme," *International Journal of Heat and Mass Transfer*, Vol. 43, No. 17, 2000, pp. 3119–3135.

Downloaded by Clinton Groth on January 1, 2022 | http://arc.aiaa.org | DOI: 10.2514/6.2022-2253

[90]McEnally, C. S., Schaffer, A. M., Long, M. B., Pfefferle, L. D., Smooke, M. D., Colket, M. B., and Hall, R. J., "Computational and experimental study of soot formation in a coflow, laminar ethylene diffusion flame," *Symposium (International) on Combustion*, Vol. 27, No. 1, 1998, pp. 1497–1505.

[91]Smooke, M. D., Hall, R. J., Colket, M. B., Fielding, J., Long, M. B., McEnally, C. S., and Pfefferle, L. D., "Investigation of the transition from lightly sooting towards heavily sooting co-flow ethylene diffusion flames," *Combustion Theory and Modelling*, Vol. 8, No. 3, 2004, pp. 593–606.

[92]Connelly, B. C., Bennett, B. A. V., Smooke, M. D., and Long, M. B., "A paradigm shift in the interaction of experiments and computations in combustion research," *Proceedings of the Combustion Institute*, Vol. 32, No. 1, 2009, pp. 879–886.

[93]Connelly, B. C., Long, M. B., Smooke, M. D., Hall, R. J., and Colket, M. B., "Computational and experimental investigation of the interaction of soot and NO in coflow diffusion flames," *Proceedings of the Combustion Institute*, Vol. 32, No. 1, 2009, pp. 777–784.

[94]Kuhn, P. B., Ma, B., Connelly, B. C., Smooke, M. D., and Long, M. B., "Soot and thin-filament pyrometry using a color digital camera," *Proceedings of the Combustion Institute*, Vol. 33, No. 1, 2011, pp. 743–750.

[95]Herdman, J. D., Connelly, B. C., Smooke, M. D., Long, M. B., and Miller, J. H., "A comparison of Raman signatures and laser-induced incandescence with direct numerical simulation of soot growth in non-premixed ethylene/air flames," *Carbon*, Vol. 49, No. 15, 2011, pp. 5298–5311.

[96]Ma, B. and Long, M. B., "Absolute light calibration using S-type thermocouples," *Proceedings of the Combustion Institute*, Vol. 34, No. 2, 2013, pp. 3531–3539.

[97]Ma, B. and Long, M. B., "Combined soot optical characterization using 2-D multi-angle light scattering and spectrally resolved line-of-sight attenuation and its implication on soot color-ratio pyrometry," *Applied Physics B*, Vol. 117, No. 1, 2014, pp. 287–303.

[98]Ma, B., Wang, G., Magnotti, G., Barlow, R. S., and Long, M. B., "Intensity-ratio and color-ratio thin-filament pyrometry: uncertainties and accuracy," *Combustion and Flame*, Vol. 161, No. 4, 2014, pp. 908–916.

[99]Kempema, N. J. and Long, M. B., "Quantitative Rayleigh thermometry for high background scattering applications with structured laser illumination planar imaging," *Applied optics*, Vol. 53, No. 29, 2014, pp. 6688–6697.

[100]Kempema, N. J. and Long, M. B., "Boundary condition thermometry using a thermographic-phosphor-coated thin filament," *Applied optics*, Vol. 55, No. 17, 2016, pp. 4691–4698.

[101]Kempema, N. J., Ma, B., and Long, M. B., "Investigation of in-flame soot optical properties in laminar coflow diffusion flames using thermophoretic particle sampling and spectral light extinction," *Applied Physics B*, Vol. 122, No. 9, 2016, pp. 1–13.

[102]Kempema, N. J. and Long, M. B., "Combined optical and TEM investigations for a detailed characterization of soot aggregate properties in a laminar coflow diffusion flame," *Combustion and Flame*, Vol. 164, 2016, pp. 373–385.

[103]Satija, A., Chang, Z., Lowe, A., Thomas, L. M., Masri, A. R., and Lucht, R. P., "CARS thermometry in laminar sooting ethylene-air co-flow diffusion flames with nitrogen dilution," *Combustion and Flame*, Vol. 208, 2019, pp. 37–44.

[104]Botero, M. L., Sheng, Y., Akroyd, J., Martin, J., Dreyer, J. A., Yang, W., and Kraft, M., "Internal structure of soot particles in a diffusion flame," *Carbon*, Vol. 141, 2019, pp. 635–642.

[105]Botero, M. L., Eaves, N., Dreyer, J. A., Sheng, Y., Akroyd, J., Yang, W., and Kraft, M., "Experimental and numerical study of the evolution of soot primary particles in a diffusion flame," *Proceedings of the Combustion Institute*, Vol. 37, No. 2, 2019, pp. 2047–2055.

[106]Dworkin, S. B., Smooke, M. D., and Giovangigli, V., "The impact of detailed multicomponent transport and thermal diffusion effects on soot formation in ethylene/air flames," *Proceedings of the Combustion Institute*, Vol. 32, No. 1, 2009, pp. 1165–1172.

[107]Khosousi, A. and Dworkin, S. B., "Soot surface reactivity during surface growth and oxidation in laminar diffusion flames," *Combustion and Flame*, Vol. 162, No. 12, 2015, pp. 4523–4532.

[108]Lindstedt, R. P. and Waldheim, B. B. O., "Modeling of soot particle size distributions in premixed stagnation flow flames," *Proceedings of the Combustion Institute*, Vol. 34, 2013, pp. 1861–1868.

[109]Aubagnac-Karkar, D., El Bakali, A., and Desgroux, P., "Soot particles inception and PAH condensation modelling applied in a soot model utilizing a sectional method," *Combustion and Flame*, Vol. 189, 2018, pp. 190–206.

[110]D'Alessio, A., Barone, A. C., Cau, R., D'Anna, A., and Minutolo, P., "Surface deposition and coagulation efficiency of combustion generated nanoparticles in the size range from 1 to 10 nm," *Proceedings of the Combustion Institute*, Vol. 30, 2005, pp. 2595–2603.

[111]D'Anna, A. and Kent, J. H., "A model of particulate and species formation applied to laminar, nonpremixed flames for three aliphatic-hydrocarbon fuels," *Combustion and Flame*, Vol. 152, No. 4, 2008, pp. 573–587.

[112]Sirignano, M. and D'Anna, A., "Coagulation of combustion generated nanoparticles in low and intermediate temperature regimes: An experimental study," *Proceedings of the Combustion Institute*, Vol. 34, No. 1, 2013, pp. 1877–1884.

[113]Chen, D., Zainuddin, Z., Yapp, E., Akroyd, J., Mosbach, S., and Kraft, M., "A fully coupled simulation of PAH and soot growth with a population balance model," *Proceedings of the Combustion Institute*, Vol. 34, No. 1, 2013, pp. 1827–1835.

[114]Sirignano, M., Ghiassi, H., D'Anna, A., and Lighty, J. A. S., "Temperature and oxygen effects on oxidation-induced fragmentation of soot particles," *Combustion and Flame*, Vol. 171, 2016, pp. 15–26.

Downloaded by Clinton Groth on January 1, 2022 | http://arc.aiaa.org | DOI: 10.2514/6.2022-2253